AD-A032 284

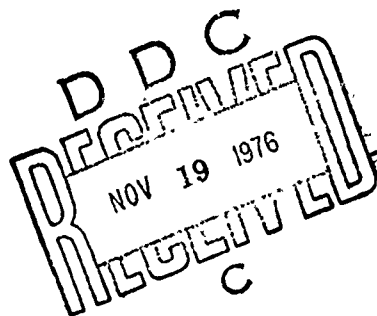# Characterization of
III-V Materials

Naval Research Lab Washington D C

Oct 76

329136

Characterization of III-V Materials

B. D. McCombe, Program Manager

Semiconductors Branch
Electronics Technology Division

October 1976

DDC

NOV 19 1976

C

NAVAL RESEARCH LABORATORY
Washington, D.C.

REPORT DOCUMENTATION PAGE		READ INSTRUCTIONS BEFORE COMPLETING FORM
1 REPORT NUMBER NRL Memorandum Report 3357	2 GOVT ACCESSION NO.	3. RECIPIENT'S CATALOG NUMBER
4 TITLE (and Subtitle) CHARACTERIZATION OF III-V MATERIALS		5. TYPE OF REPORT & PERIOD COVERED Annual summary report, 1 July 1975 — 30 June 1976
		6 PERFORMING ORG. REPORT NUMBER
7 AUTHOR(s) Bruce D. McCombe et al.		8. CONTRACT OR GRANT NUMBER(s)
9 PERFORMING ORGANIZATION NAME AND ADDRESS Naval Research Laboratory Washington, D.C. 20375		10 PROGRAM ELEMENT, PROJECT, TASK AREA & WORK UNIT NUMBERS NRL Problem P01-14C N0001476WR60035
11 CONTROLLING OFFICE NAME AND ADDRESS Office of Naval Research Electronics Program Office Arlington, Virginia 22217		12 REPORT DATE October 1976
		13 NUMBER OF PAGES 75
14 MONITORING AGENCY NAME & ADDRESS(if different from Controlling Office)		15 SECURITY CLASS (of this report) UNCLASSIFIED
		15a DECLASSIFICATION/DOWNGRADING SCHEDULE

16 DISTRIBUTION STATEMENT (of this Report)

Approved for public release; distribution unlimited.

17 DISTRIBUTION STATEMENT (of the abstract entered in Block 20, if different from Report)

18. SUPPLEMENTARY NOTES

19 KEY WORDS (Continue on reverse side if necessary and identify by block number)

Semi-insulating gallium arsenide	Photoelectromagnetic
Characterization	Galvanomagnetic
Epitaxial	Van der Pauw
Photoconductivity	Contactless
Photovoltaic	Infrared reflectance (Continues)

20 ABSTRACT (Continue on reverse side if necessary and identify by block number)

A program for the characterization of bulk and epitaxial single crystals of III-V compounds is described. The program includes electrical, chemical, structural and topographic characterization as well as device fabrication and evaluation, and is carried out on a coordinated basis by three Navy laboratories The Naval Research Laboratory, the Naval Surface Weapons Center and the Naval Electronics Laboratory Center The primary goals of the effort continue to be: (1) to provide rapid and interactive feedback of routine characterization information to the materials growth effort, and (2) to develop new, innovative methods for material characterization. Characterization techniques
(Continues)

DD FORM 1473 EDITION OF 1 NOV 65 IS OBSOLETE
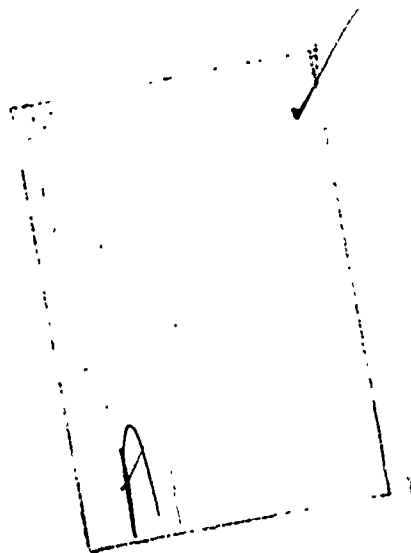1 JAN 73
S/N 0102-014-6601

i

19. Key Words (Continued)

Mobility

Carrier density

Scanning electron microscopy

Soft x-ray appearance potential spectroscopy

Photoluminescence excitation

Field effect transistor

Schottky barrier

Inhomogeneities

20. Abstract (Continued)

described include routine Hall effect measurements, photoconductivity, contactless microwave magnetoconductivity, contactless infrared optical measurements of carrier density and mobility, scanning electron microscopy, soft x-ray appearance potential spectroscopy, photoluminescence of bulk and interface states, and fabrication and test of Schottky barrier field effect transistors. Results achieved with these techniques on GaAs and InP materials produced in-house and provided by commercial laboratories are described.

CONTENTS

CHARACTERIZATION OF III-V MATERIALS

Annual Summary Report
1 July 1975 - 30 June 1976

ONR Contract N0001476 WR60035
Amendments 1 and 2

Program Manager: B. D. McCombe .

Principal Investigators:

S. G. Bishop   E. Y. Lum*
A. Clawson*   B. D. McCombe
J. W. Gibson   L. Messick*
R. J. Holm   W. J. Moore
T. A. Kennedy   E. D. Palik
W. H. Koschel   P. G. Siebenmann
R. N. Lee**   K. J. Sleger
D. Lile*   H. H. Wieder*

*NELC **NSWC

CHARACTERIZATION OF III-V MATERIALS

INTRODUCTION

The present materials characterization program is an integral
part of a coordinated growth (N000 1476WR60035) - characterization
effort directed at the development and improvement of III-V com-
pound materials (GaAs, InP) for applications in microwave devices.
The necessity for thorough characterization of semiconducting
materials for use in various electronic device applications is well
recognized; such characterization information is required for
adequate prediction of long-term device performance and reliability.
The necessary and sufficient characterization information for
the next generation of microwave devices which will utilize GaAs
or InP as not yet well established. A particular example is the
current poor control and reproducibility of commercially available
bulk semi-insulating GaAs for substrates. A knowledge of the measure-
ments required to specify "good" or "bad" substrates is completely
lacking. This program is directed at determining the necessary
material parameters (as well as suitable techniques for their
measurement) required to insure that high performance, reliable
microwave devices can be reproducibly fabricated from such charac-
terized III-V semiconductors. In these investigations it is neces-
sary to study new techniques and to utilize and develop further
existing techniques for the characterization of these materials at
all stages from initial preparation of bulk and epitaxial material
through various processing steps to evaluation of test devices.
These techniques provide electrical, chemical, and structural
information to pinpoint areas of needed improvement which can be

1

fed back to the crystal growth effort. Device fabrication and evaluation is a critical part of this integrated effort, and it is anticipated that through such a coordinated program changes in material parameters due to device processing, or direct effects of the processing on device performance can be separated from the effects of intrinsic material parameters on the device performance. During the past year such feedback from the characterization studies has proven extremely valuable in the improvement of the materials, particularly in the area of bulk growth of semi-insulating GaAs. In the coming year more emphasis will be placed on characterization of epitaxial GaAs layers, the interface between the substrate and the epi layer, and device fabrication and evaluation.

GENERAL PROGRAM

The characterization program is a coordinated effort which involves four Navy laboratories: the Naval Research Laboratory (NRL), the Naval Surface Weapons Center (NSWC), the Naval Electronics Laboratory Center (NELC) and the Naval Weapons Support Center (NWSC) Crane, Indiana. The characterization efforts are divided into three major areas: a) electrical; b) chemical, structural and topographic; and c) device fabrication and evaluation.

Much of the past year's effort has been devoted to the characterization of bulk semi-insulating GaAs. This is a natural result of a corresponding emphasis in the materials growth area as well as the recognition of the importance and impact that solution of these problems could have. Accomplishments in this area have been substantial. In addition, there has been a strong emphasis on developing and utilizing contactless characterization measurements where possible due to the obvious benefits of such nondestructive techniques. In this regard the photoluminescence technique and the microwave magnetoconductivity technique, which are described in the following, appear to be particularly promising. Techniques which provide information about large area (average) properties as well as small area properties, indicative of inhomogeneities, have been investigated. Close coordination among the various aspects of this program, as well as direct and rapid interaction with the crystal growth effort has proven to be extremely valuable. It should also be noted that this program has benefited substantially

3

from related work supported by in-house 6.1 funds at NRL, and by IR funds at NELC and NSWC(WO). Close coordination with the ONR contract research program has also been beneficial.

Progress in the various areas is reported in detail in the remainder of this report. Individual tasks (indicated by title, principal investigators, and laboratory) are grouped under the three major headings listed above. The results of mass spectroscopic analyses of bulk GaAs samples carried out at NWSC are included in the companion materials growth report.

ELECTRICAL CHARACTERIZATION

I. Electrical Optical and Photoelectrical Characterization of GaAs and InP

Principal Investigators: W. J. Moore, P. G. Siebenmann
and T. A. Kennedy, NRL

A. Introduction

The III-V compound semiconductors continue to present challenges to characterization efforts: no single characterization technique has yet been found which combines the required sensitivity with quantitative capability in easily used form. However, several techniques have been found useful and others, either singly or in combination, are being introduced into this effort.

In this section, the Hall effect, photoconductivity, infrared transmission, and magnetoconductivity efforts will be discussed. Several other useful techniques are discussed separately.

The Hall effect remains one of the most useful of all analysis techniques, in spite of its relative antiquity. In its simplest form, that is, when measurements are made at only one or two convenient temperatures, the Hall effect gives the carrier concentration (usually a measure of the net impurity concentration) and the mobility (a function of the scattering process). These pieces of information are sufficient only during the early phases of material development.

More elaborate Hall effect measurements requiring a temperature scan, can, under ideal conditions, give the activation energy of one or more impurities, their concentration, the compensating impurity concentration, and some indication of the nature of the scattering

process. However, thermally scanned Hall effect is not without practical problems. It requires that contacts be applied to the sample, it consumes a considerable amount of time, even with automated systems, and it is often incapable of identifying impurities when there are more than one or two of the same carrier type. For these reasons, the Hall effect cannot stand alone but must be supplemented by other techniques.

During the period of this report several new characterization techniques have been initiated including magnetoconductivity, photoconductivity, and infrared transmission. These techniques provide: (1) a contactless measurement of carrier mobility; (2) a sensitive technique for qualitative analysis and (3) a potential technique for quantitative analysis. Expectations that infrared transmission would be a sensitive technique for quantitative analysis have not yet been realized. The technique appears to be much less sensitive than experience with germanium would suggest. This problem is being studied but the rapid improvement in the GaAs and InP bulk material now being produced makes it questionable whether the technique will make a significant contribution to the growth effort.

Brief discussions of the present status of electrical and some optical characterization techniques are given below.

B. <u>Hall effect</u>

Routine Hall effect measurements on GaAs and InP continue to produce reliable and rapid initial characterization of samples. Efforts to improve the quality of electrical contacts have resulted in contacting procedures adequate for most single crystal samples.

Occasional semi-insulating InP crystals show some rectification but no significant problems remain.

During the period of this report, 134 samples were measured. These included samples of bulk GaAs, InP, GaAs:Cr, and InP:Fe, epitaxial GaAs, and ion-implanted GaAs.

The van der Pauw Hall apparatus is capable of measurement accuracies within $\pm$ 3% with completely well-behaved samples. However, the results are typically limited by sample related effects including inhomogeneities, surface leakage, scattering factor uncertainty, and occasional non-ohmic contacts. Samples whose resistance is as high as 5×10^9 Ω can be reliably measured.

Modifications to allow sample temperature variation from 78K to about 100°C are presently underway. No further modifications are envisioned with this system. A separate low-temperature system with continuous temperature control from 2K to 400K is being considered for detailed evaluation of n-type epilayers.

C. Photoconductivity

Infrared photoconductivity is a convenient technique for identifying accidentally introduced acceptor and, to a lesser extent, donor impurities in GaAs. Spectra of several p-type bulk samples and one p-type epitaxial sample of GaAs have been taken. All showed easily observed photoconductivity beyond the intrinsic edge. Carbon and copper have been identified in bulk samples and oscillatory photoconductivity with a period of $\sim$300cm^{-1} was observed in an epitaxial sample containing silicon impurities. Photoconductivity spectra for carbon-doped GaAs and copper-doped GaAs are given in Figures 1a and b. These spectra do not show peaks due to photoconductivity associated

witn excited states as observed by Kirkman and Stradling[1] in GaAs at about 20K as a result of the lower temperature used in these tests ($\sim$4.2K). A cold source-follower preamplifier was used for optimum sensitivity.

Photoconductivity is a useful qualitative analysis technique which is capable of identifying acceptors whose concentrations are sufficiently high (estimated $\sim 10^{13}$ cm^{-3} with the present system). It is not capable of determining the acceptor concentrations and it can detect only uncompensated acceptors (the Fermi level must lie below the acceptor). For some samples it appears to be more sensitive than photoluminescence while for other samples it appears to be less sensitive. Such differences in relative sensitivity are expected as a result of variations in the photoconductive gain, non-radiative recombination centers, and Fermi level from sample-to-sample.

D. IR transmission

Infrared absorption by transitions from impurity ground to excited states is a potential technique for quantitative impurity analysis. Absorption measurements can, if carefully performed, be used to determine the activation energy and concentration of all uncompensated impurities. Impurities with multiple levels are observed to the extent that they are uncompensated. Taking an ideal example, observation of 1 x 10^{15} cm^{-3} shallow (0.15eV) Cu states and 1 x 10^{15} cm^{-3} deep (0.45 eV) Cu states would be sufficient to demonstrate that there are 2 x 10^{15} cm^{-3} Cu impurities and at least 1 x 10^{15} cm^{-3} donors. This type of information can be determined independent of other material parameters such as dislocations,

non-radiative recombination centers, surface states, scattering centers, etc. It therefore appears to be a nearly ideal contact-free characterization technique.

Comparison of existing data for impurities in GaAs and in Ge indicate that the technique may be less sensitive in GaAs than in Ge but no more than a factor of 10 less sensitive. Germanium data for the system now being used indicate that impurity concentrations as low as 5×10^{13} cm^{-3} should be detectable in a 1 mm thick transmission sample when the impurity ionization energy, E_I, is 0.10eV. Taking a factor 10 as an estimate of the relative sensitivity for GaAs gives a sensitivity of 5×10^{14} cm^{-3} for a 1 mm sample with 0.1 eV impurities. In germanium the sensitivity varies approximately an $E_I^{-2.5}$; so taking the same variation for GaAs we predict that carbon ($E_I \stackrel{\sim}{\sim} 0.24$) should be detectable at concentrations of the order of 5×10^{13} cm^{-3}.

This expectation has not been borne out by experiment. A thick sample believed to contain about 1×10^{15} cm^{-3} carbon showed no clearly identifiable absorption. The source of the disagreement is presently unknown so efforts to clarify the problem are underway.

E. Microwave Magnetoconductivity

Microwave conductivity measurements as a function of dc magnetic field (magnetoconductivity) have been introduced as a technique for the contactless determination of carrier mobility. The technique is applicable to bulk samples but is particularly useful for epitaxial samples on insulating substrates or other thin conducting layers, e.g., ion-implanted layers. It can also be used to probe channel

9

conductivity in MIS structures by modulating the channel width.

According to the Drude model, the conductivity of charge carriers in a magnetic field varies approximately as

$$\sigma(B) = \sigma(0)\frac{1}{1+\mu^2B^2}$$

for frequencies, ω, such that $\omega \ll 1/\tau$, where τ is the carrier scattering time and $\sigma(0) = \frac{ne^2\tau}{m^*}$ with n the charge carrier density. The EM power at frequency ω is absorbed according to $P(\omega) \propto \sigma(\omega)E^2$, where E is the magnitude of the electric field of the incident EM wave. Therefore, the mobility, μ, is easily determined by fitting the measured power absorbed by an appropriate sample as a function of magnetic field to the theoretical curve. More simply, the inverse of B when $\sigma(B) = \sigma(0)/2$ gives directly the value of the mobility μ of the carriers.

This technique has been applied to bulk GaAs and InP, MOS structures in GaAs and Si, and to n-type epitaxial GaAs. In all cases the mobilities determined for bulk and epitaxial samples were in good agreement with values determined from the Hall effect. Mobilities for surface channels in MOS devices were significantly lower than bulk values and clearly showed effects due to interface scattering processes. Typical results for an n-epi layer and an ion implanted layer are shown in Figures 2a and 2b, respectively.

Careful calibration of the signal corresponding to $\sigma(\omega_c=0)$ − $\sigma(\omega_c \gg 1)$ can yield a value for the carrier density n. Such calibration measurements are currently in progress.

10

F. Future plans

Characterization of bulk and epi-layers of GaAs and InP will continue using routine techniques. Additional magnetoconductance studies of GaAs Schottkey barrier structures are planned to clarify any effects of device geometry. A deep level transient spectroscopy (DLTS) apparatus is being assembled in order to provide a capability for detection of optically inactive states in GaAs and InP. Infrared transmission and photoconductivity measurements will continue in order to determine the usefulness of transmission spectroscopy as a quantitative analysis technique. Variable temperature Hall measurements will be carried out from room temperature to temperatures in excess of 100°C in order to determine accurately the dominant impurity type and concentration in semi-insulating material.

Reference:

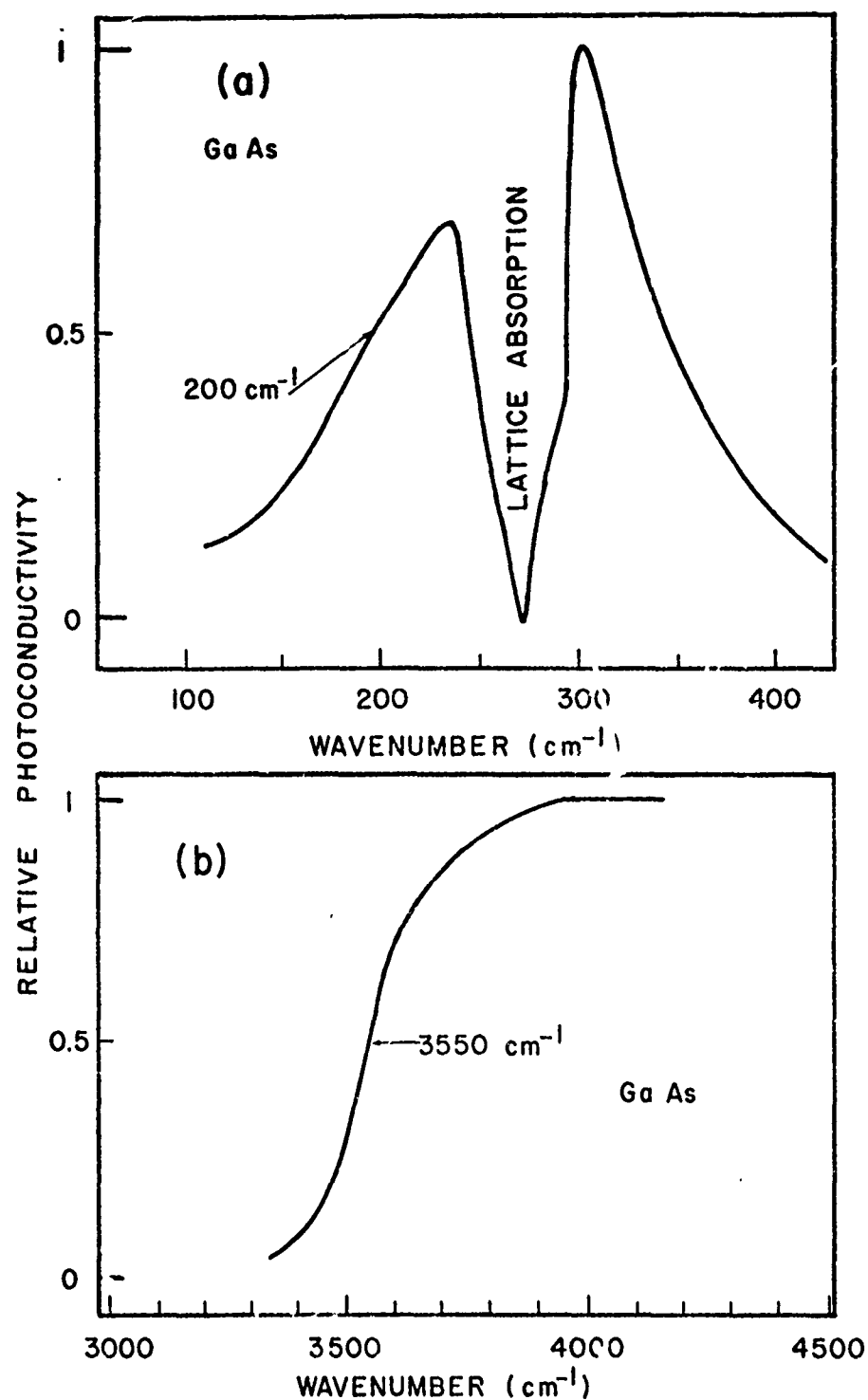[1]R. Kirkman and R. A. Stradling, Private Communications.

Fig. 1 — (a) Photoconductivity in GaAs due to an impurity believed to be carbon. The curve is not corrected for filtering which removes radiation above 300 cm^{-1}. (b) Photoconductivity in GaAs due to an impurity believed to be copper. The curve is corrected for the spectrometer characteristics.
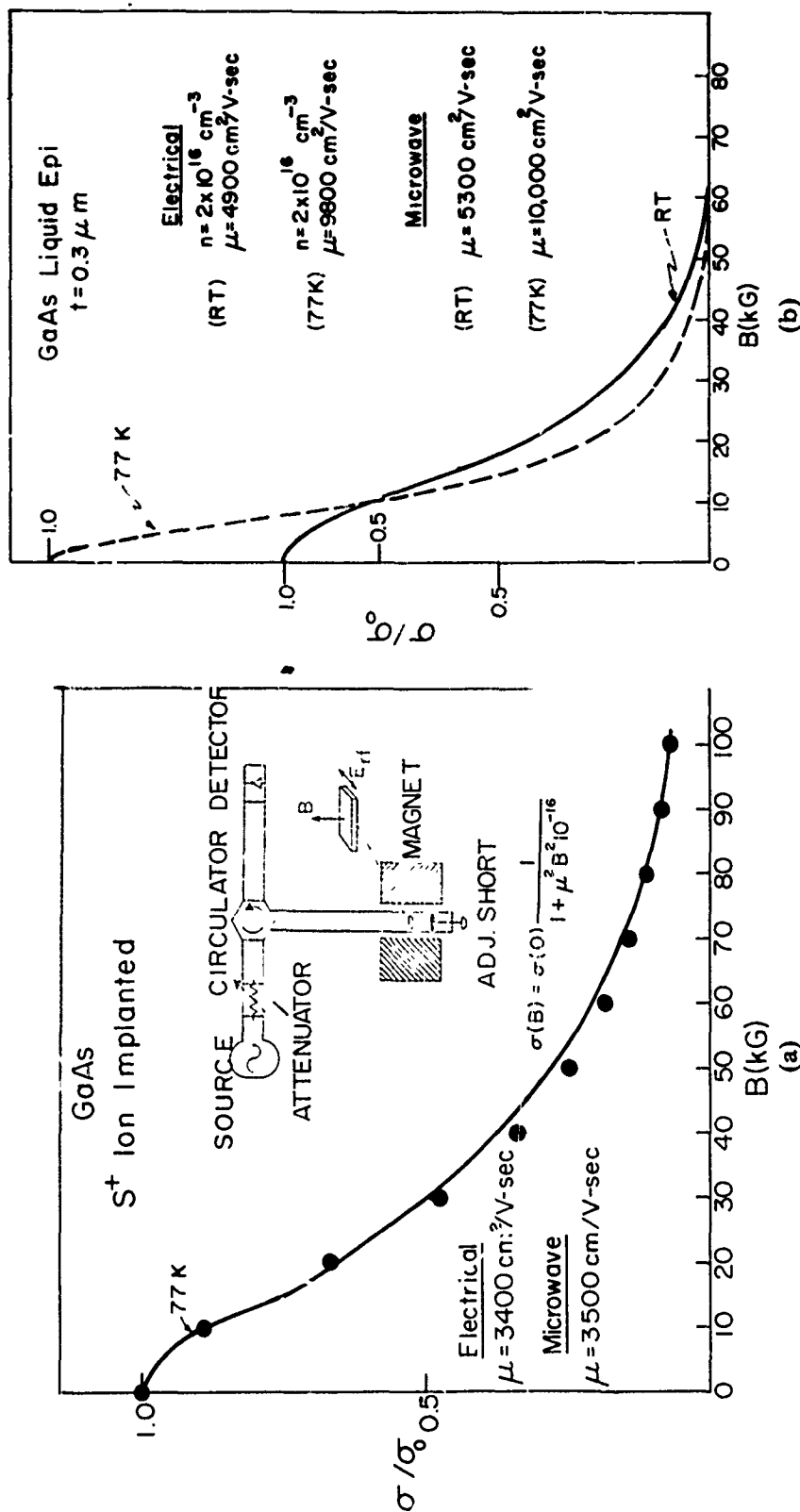
Fig. 2 — Contactless microwave mobility measurements. (a) Data (solid curve) for an n-type implanted layer on bulk semi-insulating GaAs obtained from Hughes Research Laboratories. The solid circles are the fit of the simple Drude expression for the conductivity. Microwave and van der Pauw electrical measurements are compared. The inset shows the experimental apparatus schematically. (b) Similar data at room temperature (solid curve) and 77°K (dashed curve) for an n-type liquid epitaxial layer grown in-house. Electrical and microwave measurements are compared. The microwave mobility is determined from the magnetic field at the 1/2 power point on the curve.

II. Optical (Contactless) Characterization of Thin Epitaxial Films of GaAs on GaAs Substrates

Principal Investigators: E. D. Palik, R. J. Holm, and
J. Gibson, NRL

A. Introduction

In the previous Annual Summary Report, we discussed the optical characterization of bulk GaAs samples by infrared reflectance measurements to determine the carrier density and mobility. In addition to bulk material being grown by Code 5220, thin epitaxial films of GaAs are being grown on bulk substrates. We have extended the techniques discussed previously for bulk material to these epitaxial films to characterize their carrier density, mobility and thickness.

B. Progress

The characterization of an epitaxial film on a substrate first requires the determination of the substrate parameters. The reflectance spectrum of the bulk substrate can be measured directly, the reflectance fitted with a classical dielectric-constant model, and the optical carrier density N_s and mobility μ_s determined.

Two types of epitaxial film samples have been measured: a thin, low-carrier-density film on a thick, high-carrier-density substrate (n/n+); and the reverse, a thin, high-carrier-density film on a thick, low-carrier-density substrate (n+/n). We show reflectance measurements for each type of sample in Figures 3 and 4. For the first case, Figures 3(a) and (b) show the reflectance of sample I as measured near normal incidence from the substrate and epitaxial sides of the sample, respectively. Usually, the substrate thickness is >700μm which is much greater than the penetration depth of the light, so that the substrate can be treated as bulk. The area of sample measured is a circular spot 6.3 mm in diameter.

14

The solid line in Figure 3(a) shows the least squares fit of the substrate data, from which we obtained ω_{ps} = 381.1 cm^{-1} and γ_s = 65.7 cm^{-1}. In the fitting procedure the optic-phonon parameters were taken to be (transverse phonon frequency) ω_T = 268 cm^{-1}, (longitudinal phonon frequency) ω_L = 291 cm^{-1},)phonon damping constant Γ = 1.9 cm^{-1}, and (high frequency dielectric constant) ε_∞ = 11.1. Taking into account the slight dependence of the effective mass m_s^* on N_s , one can determine N_s and μ_s from ω_{ps} and γ_s. The solid line in Figure 3(a) is a calculated spectrum for infinite resolution (infinitesimal spectral slit width), while the experimental slit widths used are shown by the vertical bars.

The fit of the reflectance from the epitaxial-film side requires a multi-layer model in which one has five adjustable parameters, ω_{ps} , γ_s for the substrate (but these are already determined) and ω_{pe} , γ_e and d (film thickness) for the epitaxial film. For the values of ω_{pe} = 0 and d - 1.18 m we obtain the fit (solid line) shown in Figure 3(b). Our fit with ω_{pe} = 0 can just barely be distinguished from a fit with ω_{pe} = 47 cm^{-1} (N_e = 2 x 10^{16} cm^{-3}) which indicates the lower limit of the sensitivity of the measurement. Thus, we conclude that in the film N_e is less than 2 x 10^{16} cm^{-3}. For this sample, the differences in the reflectance spectra of Figures 3(a) and (b) are due primarily to multiple-reflection effects in the thin film, since its free-carrier density is very low. The parameters characterizing a number of n/n+ samples are summarized in Table I.

In Figures 3(c) and (d) we show calculated reflectance spectra which demonstrate the effect of varying ω_{pe} and d, respectively, for

a fixed $\gamma_e = 60$ cm^{-1}. In Figure 3(c) the solid curve is the same as the fit in Figure 3(b). The long dashed curve and the short dashed curve are for values of $\omega_{pe} = 106$ cm^{-1} ($N_e = 1 \times 10^{17}$ cm^{-3}) and 159 cm^{-1} ($N_e = 2.2 \times 10^{17}$ cm^{-3}), respectively, with d = 1.18 µm. In Figure 3(d) the solid curve is again the fit of Figure 3(b). Now ω_{pe} is set equal to zero, and the thickness is varied to values of d = 1.4 µm (short dashed curve) and 1.0 µm (long dashed curve). The spectra are very sensitive to the film thickness. For low N_e in the film, the high frequency (say 600 cm^{-1}) reflectance is related directly to the film thickness, so a measurement here should give a precise value of d. We estimate d = 1.18 ± 0.1 µm. Scanning the sample with a small spot size would indicate the thickness variation of the film.

For the second case, sample II was a high-carrier-density film on a semi-insulating substrate. Typically, semi-insulating GaAs has N < 10^{14} electrons/cm^3, so in subsequent calculations we set $\omega_{ps} = 0$. Since the optical features of interest for this sample (film plus substrate) are nearly the same as those of a semi-insulating bulk sample, we have found it necessary to measure the ratio of the reflectance of the epitaxial-film side of sample II to the reflectance of a semi-insulating reference sample which has the same properties as the substrate of sample II.

We show in Figure 4(a) the reflectance of the (semi-insulating GaAs) reference sample. In this case, the finite resolution is taken into account in the fit by convoluting the calculated (infinite resolution) spectrum with a 2.3 cm^{-1} full-width-at-half-maximum

16

triangular slit function. Rather than use the usual literature values of ω_T, ω_L, Γ and ε_∞, we have fitted the spectrum of Figure 4(a) to obtain more precise values of these parameters, i.e., $\omega_T = 268.2$ cm^{-1}, $\omega_L = 291.5$ cm^{-1}, $\Gamma = 2.2$ cm^{-1} and $\varepsilon_\infty = 11.1$. This is necessary because the spectral features of the epitaxial-film sample are very sensitive to these parameters in contrast to the spectral features of sample I where we could use literature values.

Figure 4(b) shows the ratio of the reflectance of the epitaxial-film side (R_{EP}) to the reflectance of the reference sample (R_{SI}). This is done to emphasize the small differences. The sharp peak near 294 cm^{-1} is quite sensitive to N_e and d, but not very sensitive to μ_e. This peak is very sharp, and the fit for $\omega_{pe} = 120$ cm^{-1} shown by the dotted line includes the spectral slit-width correction and the assumption that d = 1.1 μm and $\gamma = 50$ cm^{-1}. The solid curve is the peak as calculated for infinitesimal slit width. The comparison of the optical results for several films with electrical measurements is shown in Table I. The agreement indicates that both methods are useful. In addition, the optical technique can be used to scan small areas (0.15 cm in diameter) of the epitaxial-film side of the sample to indicate the inhomogeneity of carrier density and/or film thickness.

In Figures 4(c) and (d) we show calculated reflectance spectra for infinitesimal slit width indicating the effect of varying ω_{pe} and d. In Figure 4(c) the solid curve is the same as the unconvoluted fit in Figure 4(b). We note that doubling (long dashed curve) or halving (short dashed curve) N_e for fixed d = 1.1 μm and $\Gamma = 50$ cm^{-1} causes the peak height to roughly increase or decrease a factor of two. In

17

Figure 4(d), the solid curve is again the same as the fit in
Figure 4(b). Doubling (long dashed curve) or halving (short dashed
curve) d for fixed $\omega_{pe} = 120$ cm^{-1} and $\gamma = 50$ cm^{-1} causes the peak
height to roughly increase or decrease a factor of two. Note that
comparable changes in N_e and d produce similar changes in the peak
height leading to some ambiguity in the determination of the epitaxial-
film parameters. The peak height is much less sensitive to variations
in γ_e , so that it is not possible to obtain a precise value for μ_e.
In practice, it is useful to know the thickness of the film from
another measurement such as interferometry or microscopy in order to
get an unambiguous value for ω_{pe}.

The summary of data in Table I obtained on a number of films
shows an interesting feature. In most cases the optical carrier
density tends to be less than the electrical carrier density as
obtained from CV or van der Pauw measurements. We cannot usually
fit the optical data with the electrical parameters. This apparent
discrepancy is being investigated further.

C. Plans

Preliminary measurements indicate the feasibility of scanning
n/n+ samples with a small spot size to determine the inhomogeneity
of substrate carrier density and film thickness. Similar measurements
of n+/n samples appear more difficult. These approaches will be
investigated further. The discrepancy in carrier density between
electrical and optical measurements of epitaxial films will be pur-
sued.

18

TABLE I

Optical parameters as determined from reflectance fits such as shown in Figures 3(a) and (b) and Figures 4(a) and (b). Electrical parameters are also listed where available. Bracket indicates film thickness is assumed from other value. Parentheses indicate damping constant is arbitrarily assumed.

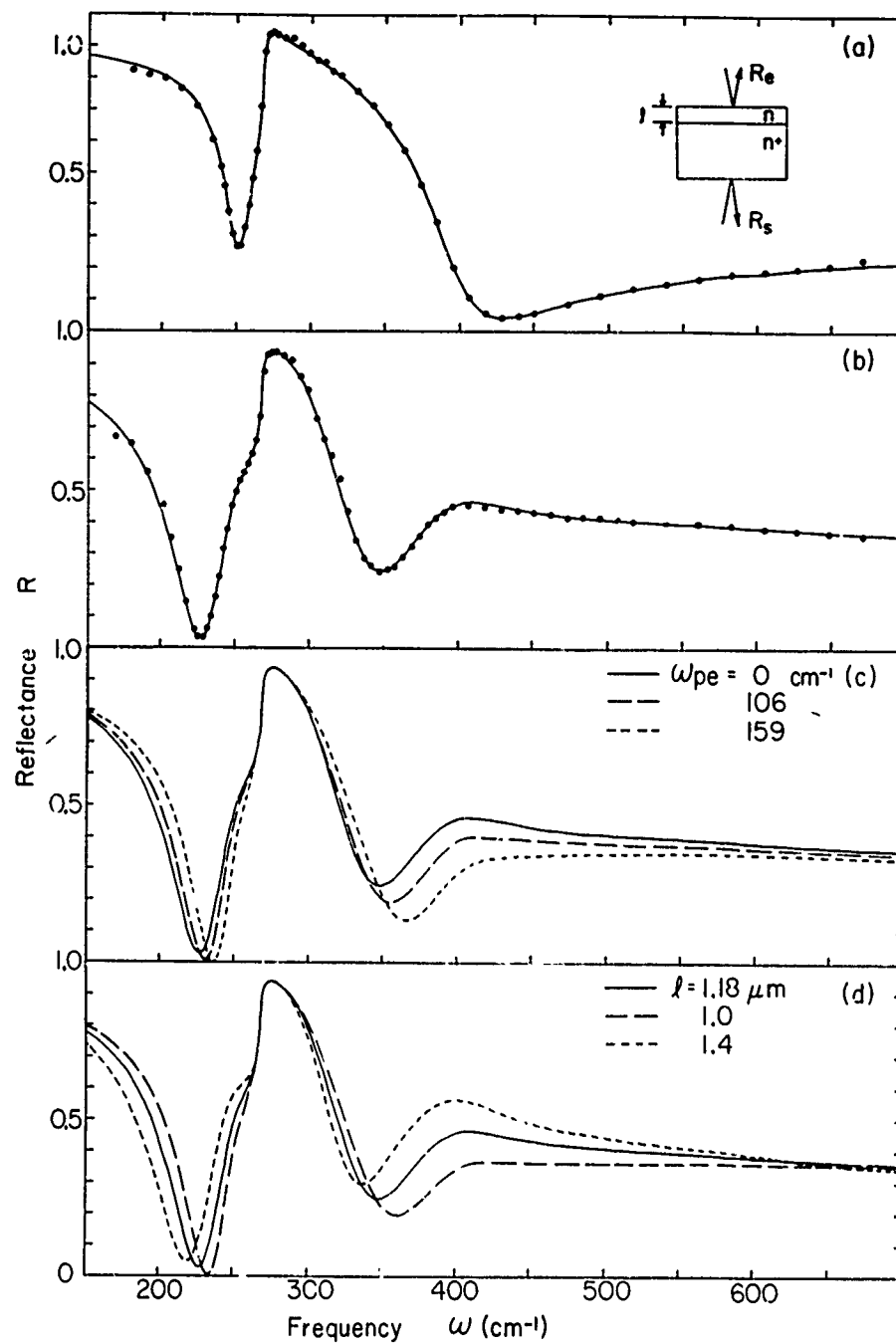|	ω_p (cm^{-1})	γ (cm^{-1})	d (μm)	N_{opt} (cm^{-3})	N_{el} (cm^{-3})	μ_{op} cm^2/Vsec	μ_{el} cm^2/Vsec	d(other) (μm)
n+/n								
subst.	0	–	–	0	–	–	–	–
film	120	(50)	1.1	1.3×10^{17}	1.2×10^{17}	(2550)	2190	1.1
subst.	0	–	–	0	–	–	–	–
film	129	(50)	1.7	1.5×10^{17}	2.8×10^{17}	(2550)	2760	1.7
subst	0	–	–	0	–	–	–	–
film	25	(30)	2.8	8×10^{15}	1.2×10^{16}	(4300)	6380	2.8
n/n+								
subst	381	66	–	1.4×10^{18}	$\sim 2 \times 10^{18}$	1850	–	–
film	<47	(60)	1.18	$<2 \times 10^{16}$	1.0×10^{17}	(2150)	–	0.5
subst.	452	70	–	1.9×10^{18}	–	1750	–	–
film	90	(50)	1.2	7×10^{16}	1.8×10^{17}	(2550)	–	1.4
subst	401	71	–	1.5×10^{18}	–	1700	–	–
film	127	46	2.9	1.4×10^{17}	1.5×10^{17}	2800	–	2.8

Fig. 3 — (a) Experimental reflectance and and calculated fit of the substrate side of Sample I. Typical spectral slit widths are shown by the vertical bars. (b) Experimental reflectance and calculated fit for the epitaxial-film side of the sample. (c) Calculated reflectance of the epitaxial film side of the sample for three values of ω_{pe} with $\gamma_e = 60$ cm^{-1} and d = 1.18 μm. (d) Calculated reflectance of the epitaxial film side of the sample for three values of d with $\omega_{pe} = 0$.
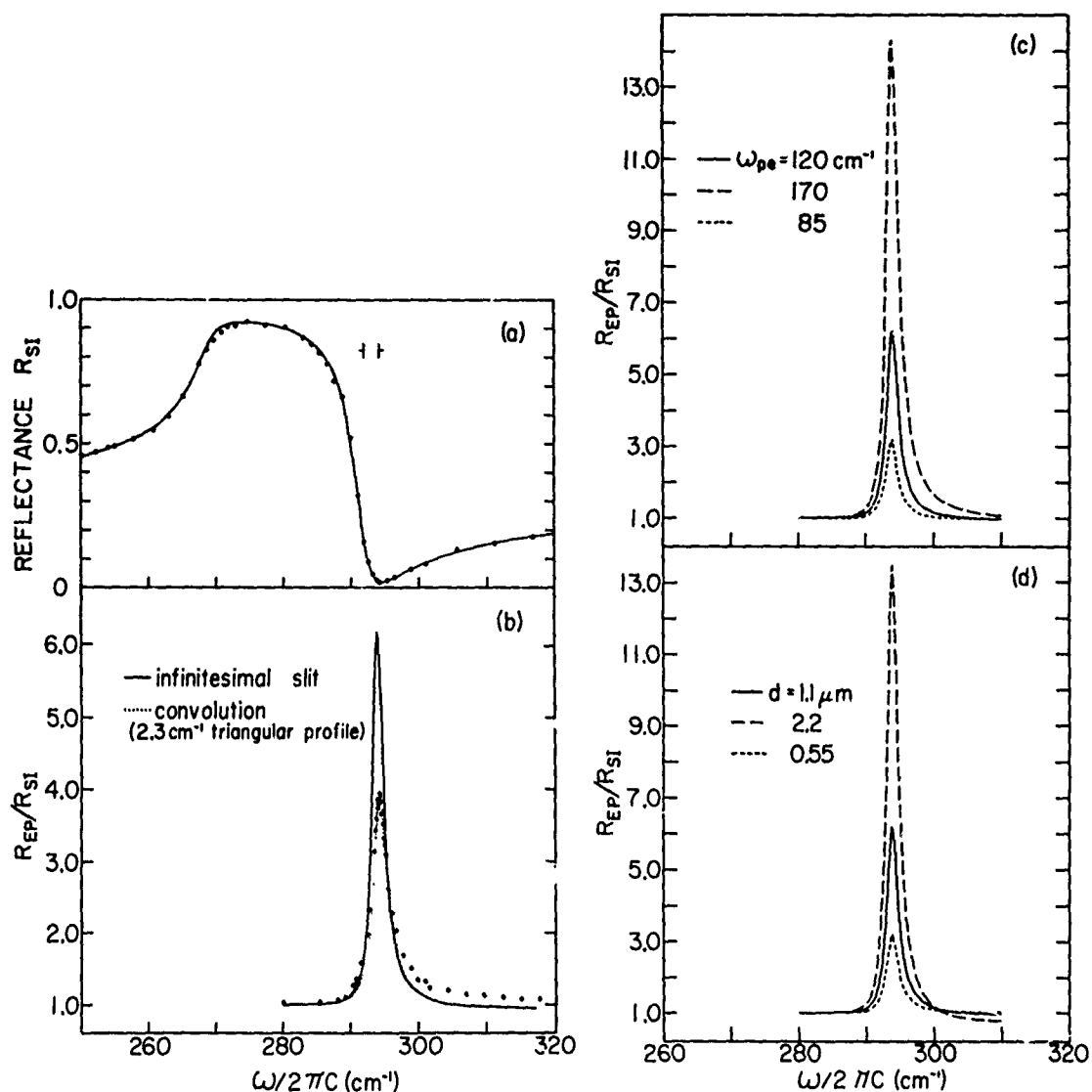
Fig. 4 — (a) Experimental reflectance and calculated fit for the semi-insulating reference sample. Spectral slit widths are shown by the vertical bars. (b) Ratio of the reflectance R_{EP} of the epitaxial-film side of Sample II to the reflectance R_{SI} of the reference sample. The calculated fit (dotted curve) is obtained by fixing $d = 1.1$ μm and $\gamma = 50$ cm^{-1}, and applying a spectral slit width correction to the solid curve to calculate the experimental line shape. (c) Calculated reflectance ratio R_{EP}/R_{SI} for three values of ω_{pe} with $\gamma_e = 50$ cm^{-1} and $d = 1.1$ μm. Spectral slit width is infinitesimal. (d) Calculated reflectance ratio R_{EP}/R_{SI} for three values of d with $\omega_{pe} = 120$ cm^{-1} and $\gamma_e = 50$ cm^{-1}.

21

CHEMICAL, STRUCTURAL AND TOPOGRAPHIC CHARACTERIZATION

I. Chemical and Topographic Characterization of the Surfaces of III-V Materials

Principal Investigator: R. N. Lee (NSWC/WO)

A. Introduction

The work on Characterization of III-V materials carried out at NSWC/WO during fiscal year 1976 included scanning electron microscope analysis of samples submitted by the Naval Research Laboratory and the development of new techniques for characterizing III-V materials. In addition to funds received from NRL, substantial support of these efforts has been provided by the Independent Research program at NSWC.

B. Scanning Electron Microscopy

One InP and five GaAs samples were submitted for SEM examination in the past year. Brief resumes of the findings for these samples is included, and a more detailed discussion of the InP sample is presented below.

1) Sample VII-45N: (100) GaAs wafer, semi-insulating Cr doped, grown and polished by Laser Diodes.

This sample was examined for chemical and topographic inhomogeneities. Gross features visible by eye and having a three dimensional appearance in SEM pictures were shown to consist solely of thin carbonaceous layers. No variation in the Ga/As ratio was detected in the SEM and impurities (Cr and Si) were found only in loose surface debris. The Siemens Electron Microprobe at the University of Maryland was used for a more sensitive examination for impurities and/or Cr inclusions. Some evidence for Cr and Si impurities was obtained at the sensitivity limit of the microprobe, but the results were non-reproducible and hence inconclusive.

2) Samples VIII-71N-1, 2 and 3; 413-III: Liquid phase epitaxial
GaAs films prepared at NRL.

These samples were submitted for SEM determination of the thick-
nesses of the epitaxial layers. Except for sample 413-III, the specimens
were fractured and etched at NRL to delineate the substrate-epilayer
boundary. In the SEM, the stained samples exhibited a multi-layered
structure. Correlation with growth conditions (i.e. the target thick-
nesses) provided positive identification of the boundaries corresponding
to the epilayer-substrate interfaces for the 1 micron and 10 micron films.
The film growth which was targeted for a 0.1 micron thickness, however,
apparently resulted only in back melting of the substrate with at most
a few patches of epilayer being deposited. The layered structure in
the 10 micron film lay entirely within the epilayer, while a layer
extending $\sim$ 20 microns into the substrate below the 1 micron film was
interpreted as an artifact of the cleavage. Sample 413-III was not
stained after cleavage and did not provide enough contrast in the SEM
for the film-substrate interface to be discernible.

3) InP Sample (1-44-H): Wafer from Fe doped material grown at NRL.

The InP wafer was submitted for compositional and topographic
analysis after etching at NRL had revealed the presence of inclusions.
The etched sample was examined in the scanning electron microscope using
secondary electron imaging, characteristic x-ray imaging and electron
microprobe analysis of selected points. Three types of inclusion were
found to protrude from the surface as a result of the differential
etching ------- whiskers, prismatic blocks and irregularly shaped
laminae.

The whiskers (Figs. 5 and 6) occurred both isolated and in patches and were by far the predominant form of inclusion. Their orientation was random with no apparent relationship to the ingot axis. The whiskers were largely of bladelike form with an inter-mixing of L-shaped cross-sections. Several isolated cases were found in which the whisker had a square cross-section with a hollow center (Figure 6). Many of the whiskers were twinned and bundles of whiskers were often found to have grown together.

The prismatic blocks were generally isolated from each other and did not appear in regions of heavy whisker growth. Figure 7 shows the typical rectangular shape and tendency toward concave irregularities. The interesting inclusion in the prism of Figure 7 can be seen to occupy a void extending from the fractured corner and emerging at the large concavity. The prisms observed were typically 50 to 100 microns in diameter.

The irregular laminae were primarily distributed in the regions of heavy whisker growth, but isolated laminae were also found. A common characteristic of the wide variety of laminar forms encountered was a tendency toward the formation of dendrites. This can be seen in the lamina shown in Figure 8.

All three types of inclusion were composed primarily of iron and phosphorous; whereas x-ray spectra from the InP matrix showed no Fe signal above background, as would be expected at normal doping levels. Characteristic x-ray imaging using the phosphorous line produced more intense images of the inclusions than of the InP matrix. This result is consistent with comparable densities of phosphorous in the two materials and a higher x-ray absorption coefficient in the InP.

The prismatic inclusions and well-formed whiskers such as that of Figure 6 contained no indium at all, being composed solely of iron and phosphorous. The blade shaped whiskers, on the other hand, produced spectra which indicated a variable indium content in the range of 10% of that in the InP matrix. However, there was evidence that these In spectral lines were at least partially due to secondary scattering from the InP matrix. In contrast with this, variable composition of the irregular laminae was quite definite. The relative heights of the spectral lines for In, P and Fe varied widely from point to point on a given lamina, and regions were found which were composed almost entirely of indium.

The composition of the inclusion in the prism of Figure 7 proved to be of special interest. By far the strongest line in the spectrum from a point on the inclusion was that of Fe. The next highest peak was due to Cu, and there were weak peaks from In, P and Al. The In and P peaks were probably due to secondary scattering from the InP matrix, and the Al peak may have come from an aluminum collar surrounding the sample. The copper peak was too strong to be explained away in this manner, however. A spectrum taken from a point on the prism just adjacent to the inclusion showed no indication of elements other than iron and phosphorous.

We conclude from the spectra and structural forms that the whiskers and prisms are crystallites of an iron-phosphorous compound (probably FeP, which is rhombohedral) which formed around iron precipitates in the melt. The laminae are of mixed phase and appear to have formed in regions of relatively dilute condensation of the iron.

C. Soft X-Ray Appearance Potential Spectroscopy (SXAPS)

We have now completed the development of the high sensitivity SXAPS instrument which was outlined in the previous annual report. The present instrument easily meets our goal of good signal-to-noise at low power inputs. Conventional SXAPS spectrometers have been effectively limited to the study of metals and refractory materials due to the necessarily high power input to the sample. The two to three order of magnitude reduction in power which we have now realized makes possible the application of SXAPS to the study and characterization of compound semiconductors.

The SXAPS technique is a core-hole spectroscopy which provides much the same information as does ESCA, but it offers the advantages of higher energy resolution, substantially lower cost and ease of use as an add-on instrument on a vacuum chamber. Briefly, in SXAPS the sample is bombarded with electrons of energy E_i and the soft x-rays produced are detected. At energies below 2 keV (an arbitrary upper limit on most SXAPS studies), the x-ray flux is linear with E_i except for small abrupt increases at the threshhold energies E_A for ionization of atomic core levels in the solid. Modulation techniques are used to obtain derivative spectra from which the E_A (i.e. the core level binding energies) can be directly and precisely determined.

Since SXAPS measures the binding energies E_A directly rather than just the term differences provided by Auger Electron Spectroscopy, it offers the advantage over AES of determining the first order chemical shifts due to changes in bonding and provides an easier elemental analysis of the sample. In addition, the line shape is directly related to the local density of states at the Fermi level, and SXAPS thus provides a fairly direct picture of

the electronic configuration at the individual atomic sites.

The absence of dispersive energy analysis in SXAPS (in effect, the E_A are measured with a voltmeter) results in it having the highest energy resolution of any of the core hole spectroscopies. In most cases, the fundamental limit imposed on the energy resolution by the natural width of the core level is realized.

The SXAPS spectrometer we have developed is depicted schematically in Figure 9. Soft x-rays produced by electron bombardment of the sample impinge on the front surface of a Channelplate Electron Multiplier Array (CEMA) where they produce photoelectrons. The CEMA then multiplies this photocurrent, producing a shower of 10^4 electrons out of its back surface for each photoelectron. The amplified current is collected on a plate and the part of the signal which is synchronous with the sample potential modulation is detected across an L-C tank circuit.

The improvement over the conventional SXAPS spectrometer employing a gold photocathode is illustrated graphically in Figure 10. The conventional instrument must normally be operated at an electron bombardment current of 1 to 10 mA for good signal-to-noise, and the 10 µA spectrum of Figure 10 represents a two to three order of magnitude reduction in power to the sample. Figure 11 is a more complete first derivative spectrum of NiTi taken with a primary current of 50 µA.

The essential improvement stems from the relatively high quantum efficiency of the CEMA in the soft x-ray range as compared to the gold photocathode. The ultimate limit of sensitivity is determined

by the signal-to-shot-noise ratio, and shot noise is most directly reduced at a given x-ray flux by improving the quantum efficiency of the detector. The CEMA also provides a less fundamental advantage in that the signal multiplication makes it much easier to eliminate Johnson noise.

A further improvement in signal-to-noise can be effected by the use of a thin Al filter in front of the CEMA to reduce the amount of low energy brehmstrahlung contributing to the shot noise. No filter was used in taking the spectra of Figures 10 and 11.
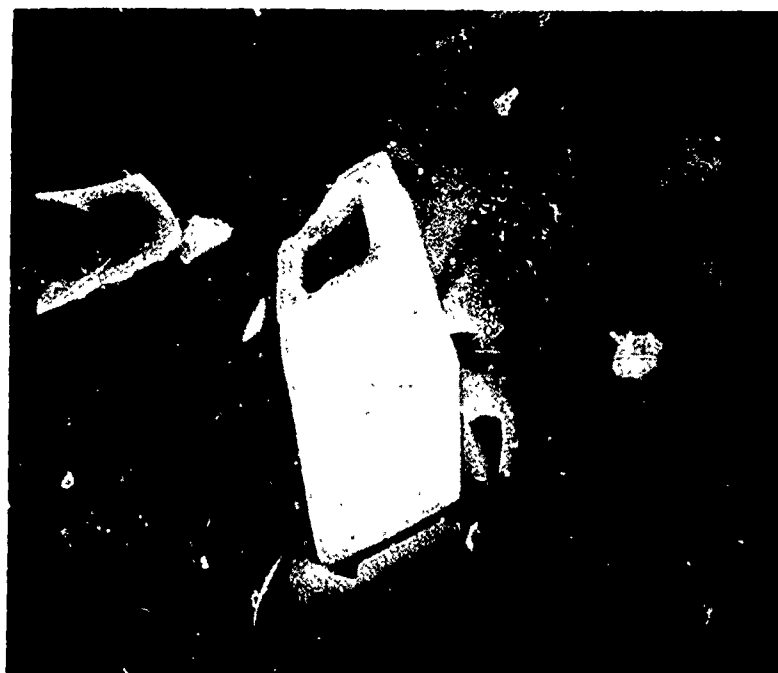
D. Plans

The Solid State Branch (WR-34) of NSWC/WO has recently adopted a policy of emphasizing the study and characterization of GaAs and other III-V materials. Work is now under way or will soon begin on surface properties, metal-semiconductor interfaces, magnetophonon interactions, high field transport, cathodoluminescence and proton induced fluorescence. This effort will be strongly coordinated with the programs at NRL and other Navy laboratories. The present program on Characterization of III-V Materials funded through NRL will become an integral part of the larger III-V effort at NSWC/WO and will benefit from the wider range of resources that this implies.

In addition to providing SEM analysis of samples submitted in the coming year, we will explore the range of information which SXAPS can provide about the III-V semiconductors. Development of the new spectrometer was necessarily carried out with metal samples, and at the present time no detailed SXAPS studies of compound semiconductors exist. The field is thus entirely unexplored and promises to be richly rewarding.

28

$\vdash\!\!\dashv$
10μ

Fig. 5 — Whiskers protruding from an iron-doped InP wafer after etching. These whiskers represent inclusions in the InP wafer which are revealed by differential etching.

4μ

Fig. 6 — A hollow whisker protruding from an InP wafer after etching. This whisker represents an inclusion in the InP wafer which is revealed by differential etching.
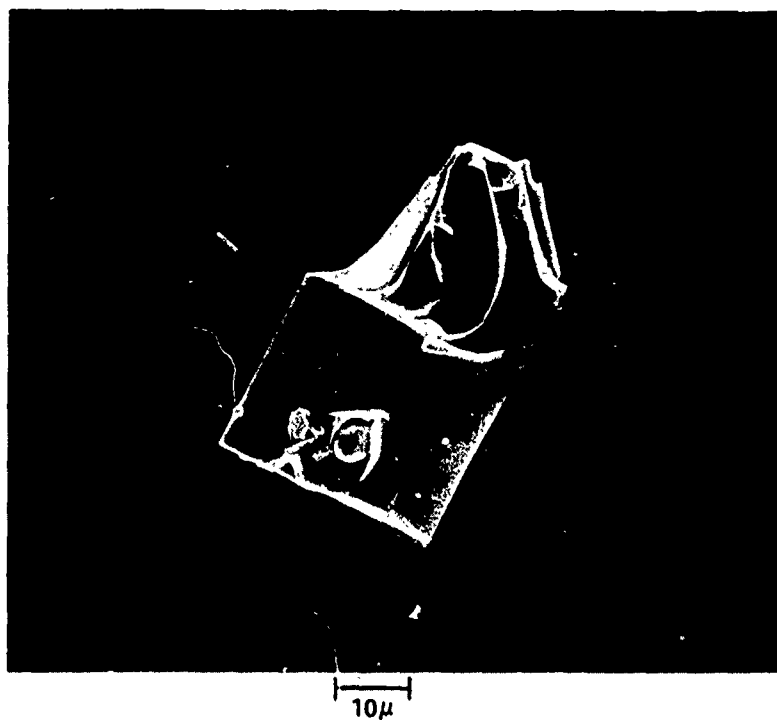
10μ

Fig. 7 — A prismatic block inclusion in an InP wafer which
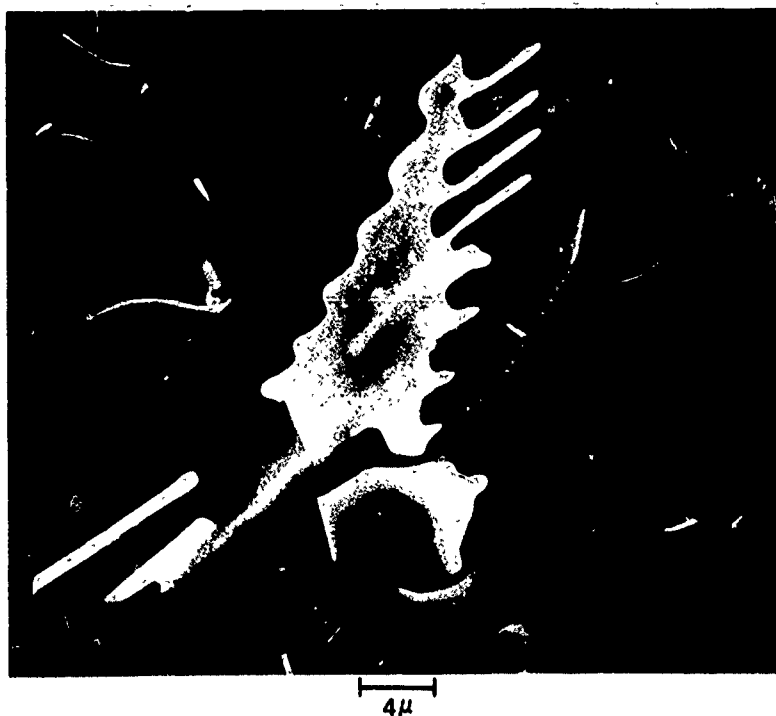itself contains a cylindrical inclusion

Fig. 8 — An irregularly shaped laminar inclusion in an InP wafer. This laminar inclusion shows dendritic formation.
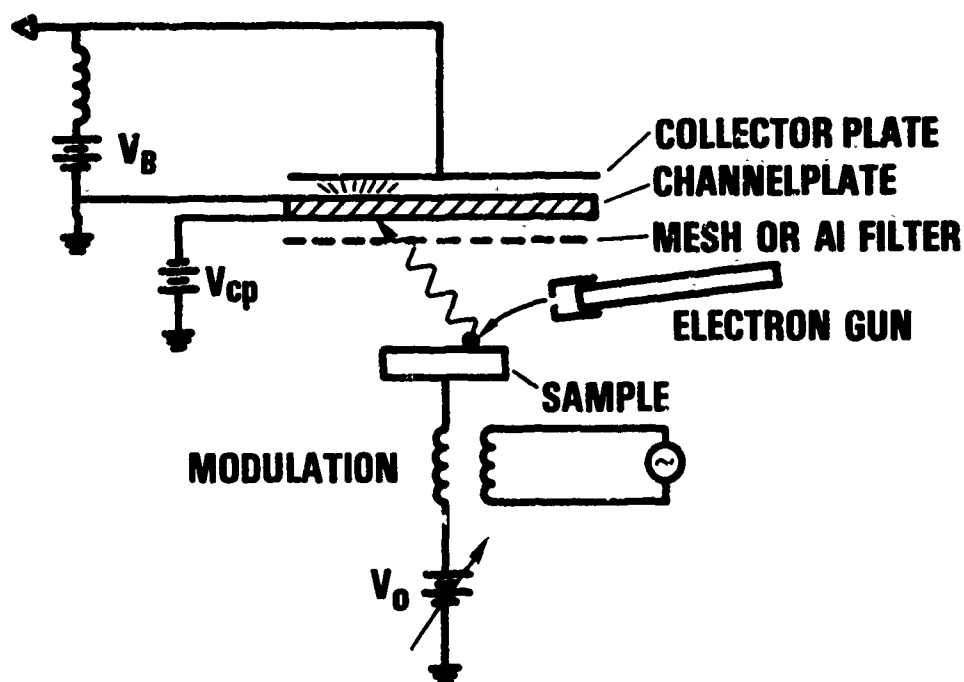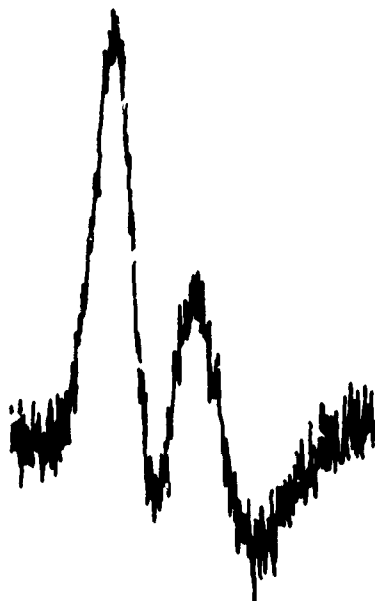
Fig. 9 — Schematic representation of the channelplate SXAPS spectrometer. Soft x-rays produced by electron bombardment of the sample produce photoelectrons from the front surface of a channelplate electron multiplier with a gain of 10^4. The amplified signal is collected at the collector plate and measured by a tuned synchronous detector.

SXAPS: TITANIUM L_2, L_3 LINES AT Ipr = 10μA.
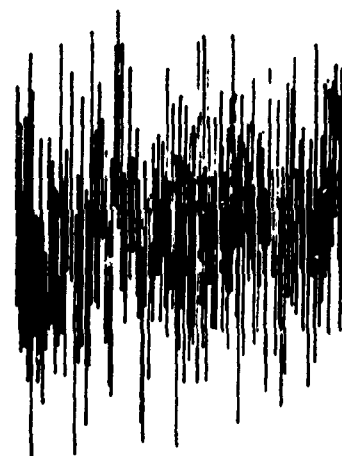
CHANNELPLATE   **Au PHOTOCATHODE**

Fig. 10 — Performance of channelplate and conventional gold photocathode
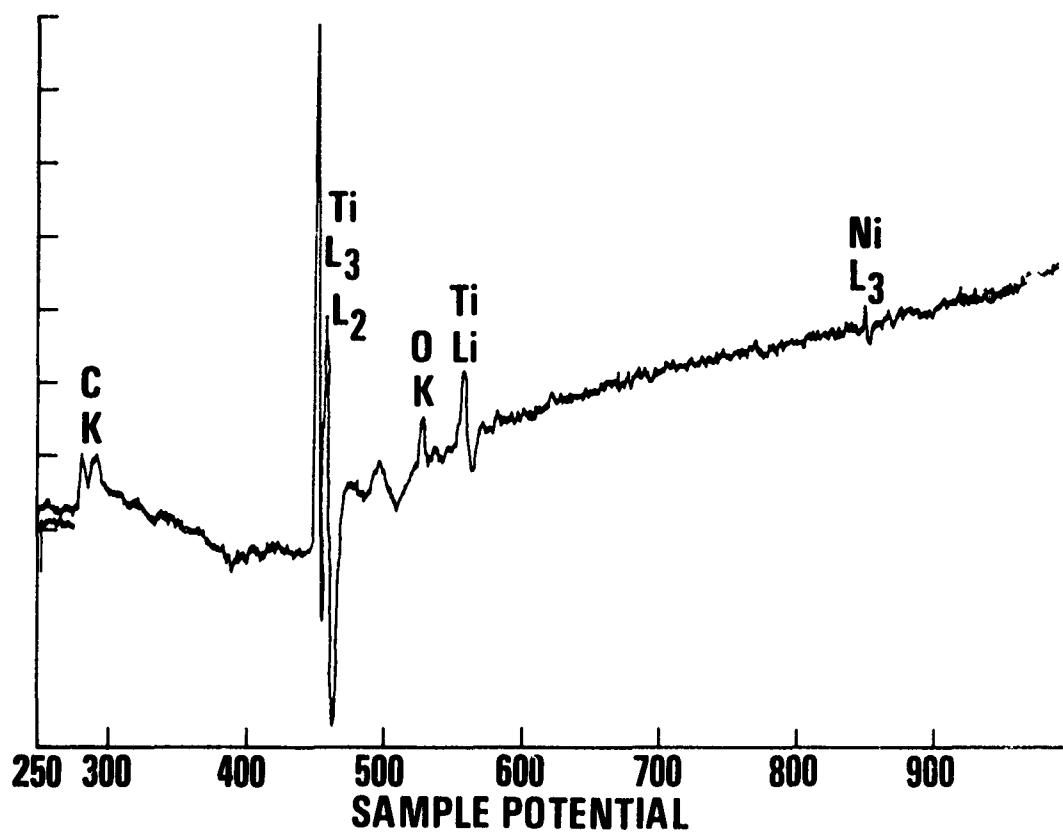SXAPS spectrometers at an electron bombardment current of 10 μA

SXAPS — NiTi

Fig. 11 — Performance of the channelplate SXAPS spectrometer with a NiTi sample at 50 μA electron bombardment current in the derivative mode

II. Photoluminescence Characterization of Bulk and Interface Properties of GaAs and InP

Principal Investigators: S. G. Bishop, W. H. Koschel and B. D. McCombe, NRL

A. Introduction

In the year since the previous Annual Summary Report the capabilities of photoluminescence (PL) apparatus have been greatly improved by the acquisition of a Krypton laser, a new 3/4 meter (Czerny-Turner grating monochrometer, a liquid nitrogen cooled PbS photoconductive cell, and a high sensitivity cooled S-1 surface photomultiplier tube. This detection system has a greatly improved sensitivity throughout the 1.5 to 0.3 eV spectral range permitting the observation of weaker signals at better resolution. The Krypton laser provides much higher excitation intensities and relieves the problem of stray exciting light in the spectral range of the luminescence encountered with broad band excitation sources.

The improved capabilities of the photomultiplier system have allowed us to identify on a routine basis the shallow acceptors in bulk and epitaxial GaAs through the observation of the free-to-bound luminescence transitions in the near band edge spectral range (1.5-1.2eV). Vacancy-acceptor complex bands have also been studied in this spectral range. Correspondingly, the improved sensitivity of the cooled PbS detector has enabled us to make detailed studies of the PL spectra from deep transition metal impurities such as Cr and Fe in GaAs and InP.

B. Progress and Current Status

1. Samples Studied

PL characterization studies have been carried out on samples of

36

semi-insulating bulk GaAs obtained from Laser Diodes, Inc., Monsanto, Crystal Specialties, Siemens A. G., Stanford Univ., as well as a variety of GaAs and InP samples grown in house by Code 5220. Most of the samples from commercial suppliers were Cr-doped while the in house samples included Cr-doped, O-doped, Fe-doped, and high-purity undoped material compounded and pulled in pyrolytic boron nitride crucibles. In addition, several LPE grown layers of GaAs provided by Stanford Univ. have been studied.

2. Identification of Shallow Impurities

Studies of the near band edge PL in GaAs have identified the bound exciton transition and the so-called free-to-bound radiative transitions involving a variety of shallow acceptors (Zn, C, Si, Ge, etc.). Comparison of the PL peak energies with standard references[1] enables the shallow acceptor present to be identified. Thi service has been supplied on a routine basis to the in-house crystal growth effort. The spectral widths of these exciton bound impurity PL ions also provide a rough indication of crystal quality. A typical near band edge PL spectrum is shown in Figure 12.

3. Identification of Deep Impurities

As in the case of shallow acceptors, comparison of "deep" PL bands observed in various samples of GaAs with standard references[2-5] often permits the identification of the deep impurity. In Figure 13 the deep PL spectra from several samples are presented with PL bands attributed to Cr, Fe, and Oxygen impurities. These bands are first identified in purposely doped samples which can then serve as standards for comparison with samples under analysis. The PL band observed at 0.8eV in GaAs-Cr has been attributed to Cr by other

authors[2,3] and we have found its intensity to correlate with Cr
content over a wide range of doping concentrations. This band is
generally accompanied by a deeper band at 0.56 eV which we also
attribute to Cr. Other workers[4] have identified the band at about
0.65 eV as an oxygen band. We have observed this band weakly,
apparently as an unintentional dopant, in several samples; it was
quite strong in two oxygen doped samples confirming its identifica-
tion as an oxygen band. The sharp line at 0.37 eV in the Stanford
LPE sample (Figures 13 and 14) corresponds to a sharp absorption line
observed[5] at 0.37 eV in GaAs:Fe. Furthermore, we have observed[8]
(Figure 14) a similar spectrum near 0.35 eV in InP:Fe. These bands
are therefore attributed to Fe and will be discussed further in the
next section.

4. Interpretation of Deep Transition Metal Impurity PL
   Spectra in III-V Compounds

A portion of the PL spectrum observed in semi-insulating bulk
GaAs:Cr at 6K is shown in Figure 15. This 0.8 eV band is attributed
to the presence of Cr and the sharp zero phonon line at 0.837 eV
has been assigned to intracenter transitions between the ^5E and
$^5T_2$ crystal field levels of Cr^{2+} in tetrahedral coordination.[6-8]
This zero phonon line was also observed in low resistivity n-type
LPE grown GaAs doped with Cr,[6-10] and it provided the first indica-
tion that recombination at the deep transition metal impurity
levels is characterized by intracenter transitions within the d-
shells of the dopant rather than band-acceptor or donor-acceptor
recombination which is observed for shallow acceptor luminescence.

Another characteristic feature of the PL from deep centers is the strong phonon coupling which produces the phonon replicas or phonon side bands seen in Figure 15 on the lower energy side of the zero phonon line. The shape of these phonon side bands can be explained by the coupling of the TA(X) and LO(Γ) phonons to the deep acceptor levels. The coupling of the zone boundary TA phonon is larger than the coupling of the LO phonon; this behaviour is in contrast to the recombination at the shallow acceptor levels where the coupling to the LO(Γ) phonon dominates the phonon replica bands. In InP:Cr a corresponding PL band is observed at about 0.85 eV (Figure 15). It too exhibits evidence of a zero phonon line and a low energy phonon side band.

The additional "Deeper" PL band observed at 0.56 eV in GaAs:Cr has been tentatively assigned to a transition at Cr^{3+} sites.[6-9]

The PL spectra attributed to Fe in GaAs and InP are shown in Figure 14. Fe-doped InP exhibits a PL band at 0.35 eV with four well resolved zero phonon lines (the splitting is 2 meV). These PL lines are probably attributable to transitions between the $^5T_2$ and ^5E crystal field levels of Fe^{2+} in tetrahedral coordination. The ^5E groundstate is split into five levels and the PL transitions would occur from the lowest excited state $\Gamma_5(^5T_2)$ to Γ_5, Γ_3, Γ_4, $\Gamma_1(^5E)$ of the ground state. A phonon side band involving coupling of the TA zone boundary phonon is also observed in the PL spectrum.

As mentioned above, a similar PL band at 0.37 eV was observed in a GaAs liquid epitaxial layer which was not intentionally iron doped (Figures 13 and 14). However, the two strongest PL lines are

found to coincide with absorption lines of GaAs:Fe[5] which have been attributed to the $\Gamma_1(^5E) - \Gamma_5(^5T_2)$ and $\Gamma_4(^5E) - \Gamma_5(^5T_2)$ transitions of Fe^{2+} in tetrahedral coordination. The observed PL spectrum is therefore interpreted as representative of Fe doped GaAs.

The observed zero phonon lines in the PL spectra of Fe-doped III-V compounds provide further evidence that radiative recombination at deep transition metal acceptor levels is characterized by intracenter transitions rather than by the band to acceptor level transitions observed for shallow acceptors in these materials.

5. PL Studies of Surface Degradation on Semi-Insulating GaAs Substrates during the LPE Growth Cycle

It has been demonstrated previously that when a semi-insulating GaAs substrate is heated to LPE growth temperature a conducting layer can be formed on its surface.[11] We have used PL techniques to detect and characterize such type-converted surface layers.[12] Both high purity and Cr-doped semi-insulating GaAs substrates have been studied before and after heat treatment at 740^OC for 100 min. After heat treatment (annealing) in the LPE reactor the surface exhibits a strong carbon shallow acceptor PL line at 1.491 eV and an additional defect-related PL band at 1.413 eV (Fig. 16a and b). We have also observed (Fig. 16c) that a liquid gallium etch[13] of the heat treated substrate greatly reduces the intensity of the carbon shallow acceptor PL and removes the defect band at 1.413 eV, indicating that these PL features are characteristic of a surface layer only. A possible explanation of these changes in the PL spectrum is that heat treatment of the substrate leads to the formation of arsenic vacancies at the surface

which diffuse into the bulk. Carbon atoms either present in the substrate or also diffusing in during the heat treatment occupy the arsenic vacancies and give rise to the 1.491 eV shallow acceptor PL line while the 1.413 eV band is attributed to carbon atom-arsenic vacancy complexes. Additional details of similar collaborative work carried out at NELC are presented in Section III.

C. Future Plans

During the coming year, a significant amount of experimental effort will continue to be devoted to the routine identification by PL techniques of shallow and deep impurities in GaAs and InP grown in house. An attempt will be made to enhance this service capability by establishing standard samples with known impurity concentrations whose PL spectra can be compared with uncharacterized samples in order to provide a semi-quantitative estimate of the luminescent impurity concentration. Such information would be extremely useful for evaluation of crystal growth procedures.

The study of the type-converted surface layer in heat treated semi-insulating GaAs will continue. Anodic oxidation and stripping with subsequent PL and transport measurements will be used to determine the thickness of the conducting surface layer. In addition, substrates annealed in an arsenic atmosphere will be studied to test the arsenic vacancy diffusion hypothesis, and an attempt will be made to determine the source of the carbon deposits appearing in the surface layer.

The studies of the intracenter PL transitions observed for CR and Fe dopants in GaAs and InP will continue. A search for a deeper PL band associated with Fe^{3+} will be carried out in Fe-doped InP

and GaAs. In addition, the deep ($\sim.35eV$) Fe^{2+} PL band should permit extrinsic excitation spectra to be obtained for the entire spectral range from the band edge down to $\sim0.4eV$ in Fe-doped samples, thus affording the opportunity to study the extrinsic absorption by the deep chromium and oxygen impurity centers.

Publications

The PL work carried out to date has been or will be published in Bull. Am. Phys. Soc. (ref 6, Denver Am. Phys. Soc. Meeting), Solid State Communications (ref 7), in the Proceedings of the XIII Intl. Conf. on Physics of Semiconductors (ref 8, Rome, Sept 1976), and the Proceedings of the Intl. Symposium on Gallium Arsenide and Related Compounds (ref 12, Edinburgh, Sept 1976).

References

1. D. J. Ashen, P. J. Dean, D. T. J. Hurle, J. B. Mullin, and A. M. White, J. Phys. Chem. Solids 36, 1041 (1975).

2. G. A. Allen, Brit. J. Appl. Phys. 1, 593 (1968).

3. G. P. Peka and Yu. I. Karkhanin, Sov. Phys. Semicond. 6, 261 (1972).

4. W. J. Turner, G. O. Pettit, and N. G. Ainsle, J. Appl. Phys. 34, 3274 (1963).

5. J. M. Baranowsky, J. W. Allen, and G. L. Pearson, Phys. Rev. 160, 627 (1967).

6. W. H. Koschel, S. G. Bishop, and B. D. McCombe, Bull. Am. Phys. Soc. 21, 251 (1976).

7. W. H. Koschel, S. G. Bishop, and B. D. McCombe, Solid State Commun., 19, 521 (1976).

8. W. H. Koschel, S. G. Bishop, and B. D. McCombe, Proc. XIII
    Intl. Conf. on Physics of Semicond., Rome, Italy, Sept 1976.

9. The Cr is believed to be substitutional for Ga. The notation
    Cr^{2+} and Cr^{3+} refers to the $3d^4$ and $3d^3$ configurations at the
    Cr. However, the 3d-like wavefunctions of the excited states
    may contain a considerable admixture of the ligand wavefunctions
    due to covalent bonding. Thus the crystal-field description may
    not be completely adequate.

10. H. J. Stocker and M. Schmidt, J. Appl. Phys. <u>47</u>, 2450 (1976).

11. J. Barrera, Proc. Cornell EE Conf. on Active S.C. Devices for
    Microwave and Integrated Optics, Cornell U. Coll of EE, Vol. 5,
    p. 135 (1975).

12. W. H. Koschel, S. G. Bishop, B. D. McCombe (NRL), L. W. Lum and
    H. H. Wieder (NELC, San Diego), Proc. Intl. Symposium on GaAs
    and Rotated Compounds, Edinburgh, Sept 1976.

13. P. Nordquist, H. Lessoff, and E. M. Swiggard, Mat. Res. Bulletin
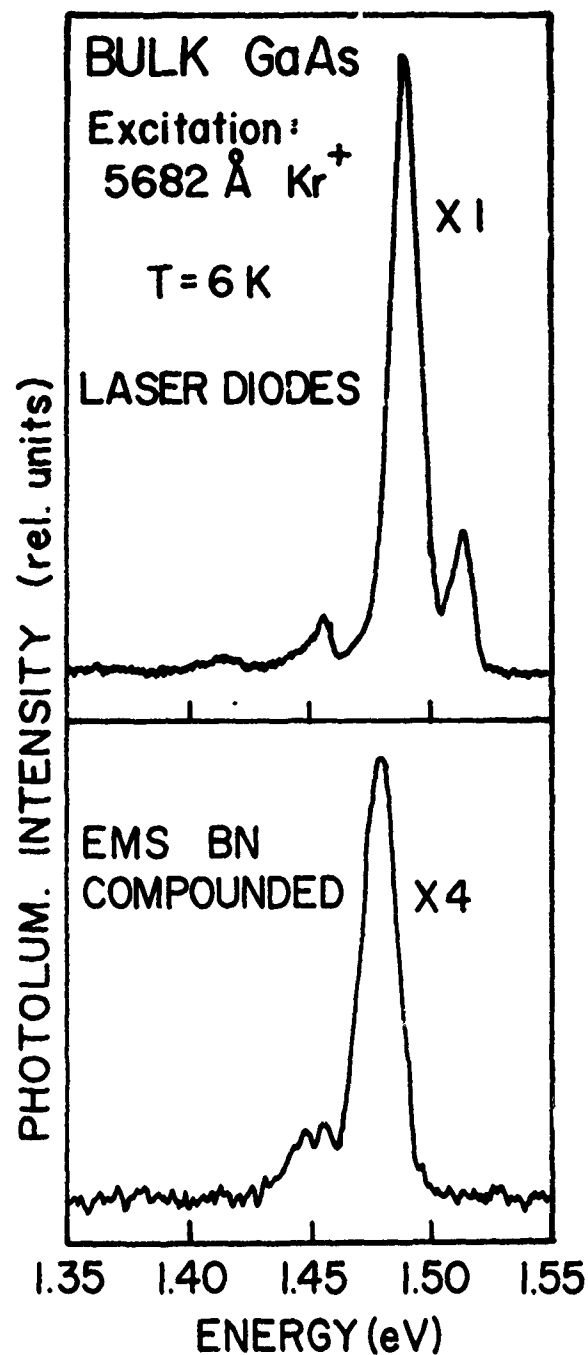   (1976) Submitted.

Fig. 12 — Top spectrum is near band edge PL from bulk GaAs crystal supplied by Laser Diodes, Inc. Strong peak near ~ 1.49 eV is attributed to Si shallow acceptors while the ~ 1.51 eV line is the bound exciton. Bottom spectrum is the same energy range for high purity bulk GaAs grown at NRL in BN. The PL line at ~ 1.48 eV is tentatively attributed to trace amounts of Ge shallow acceptors.
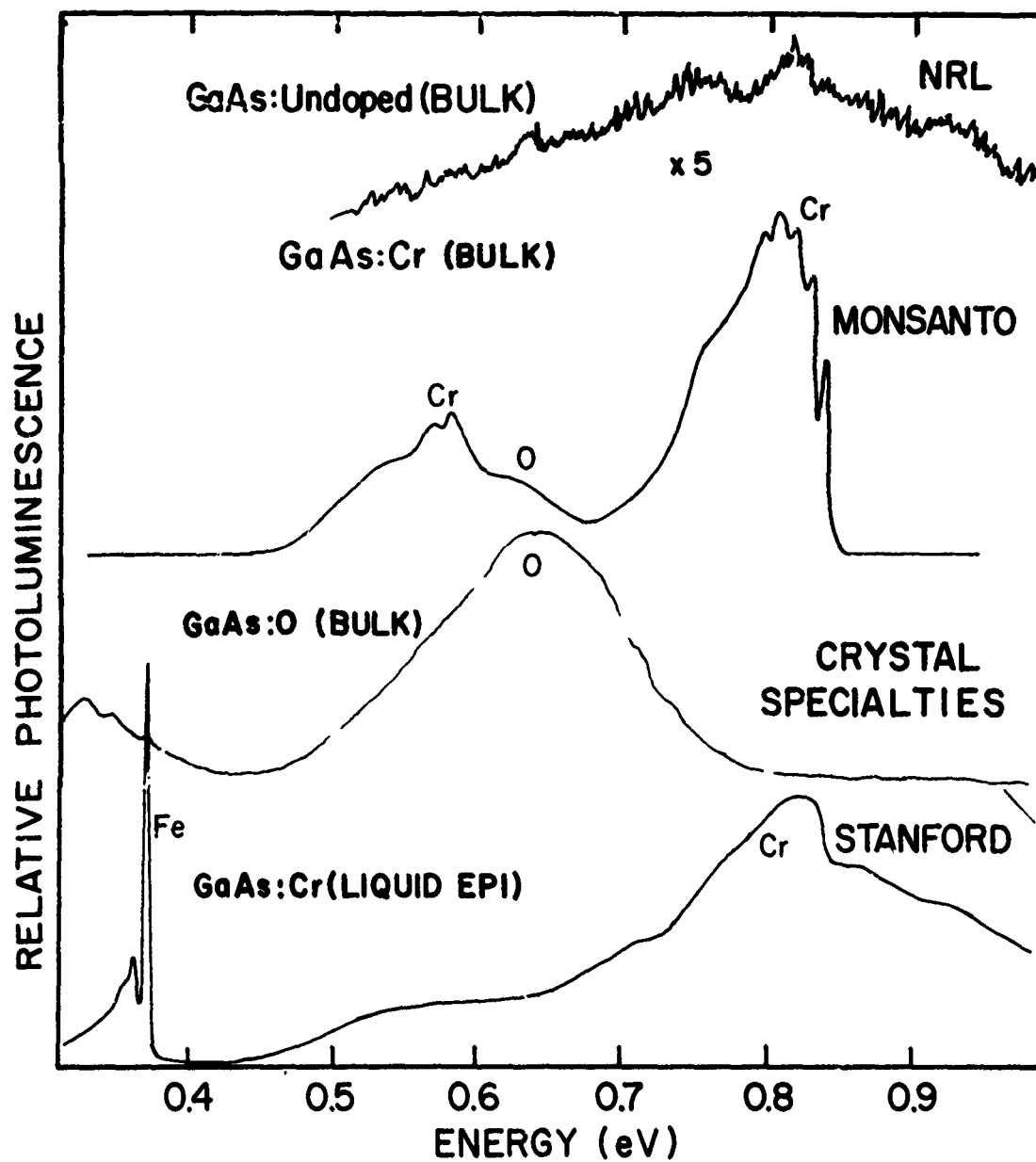
Fig. 13 — "Deep" PL spectra from GaAs samples doped with Cr, O, and Fe. Topmost spectrum represents background level of PL in undoped or high purity bulk GaAs grown at NRL.
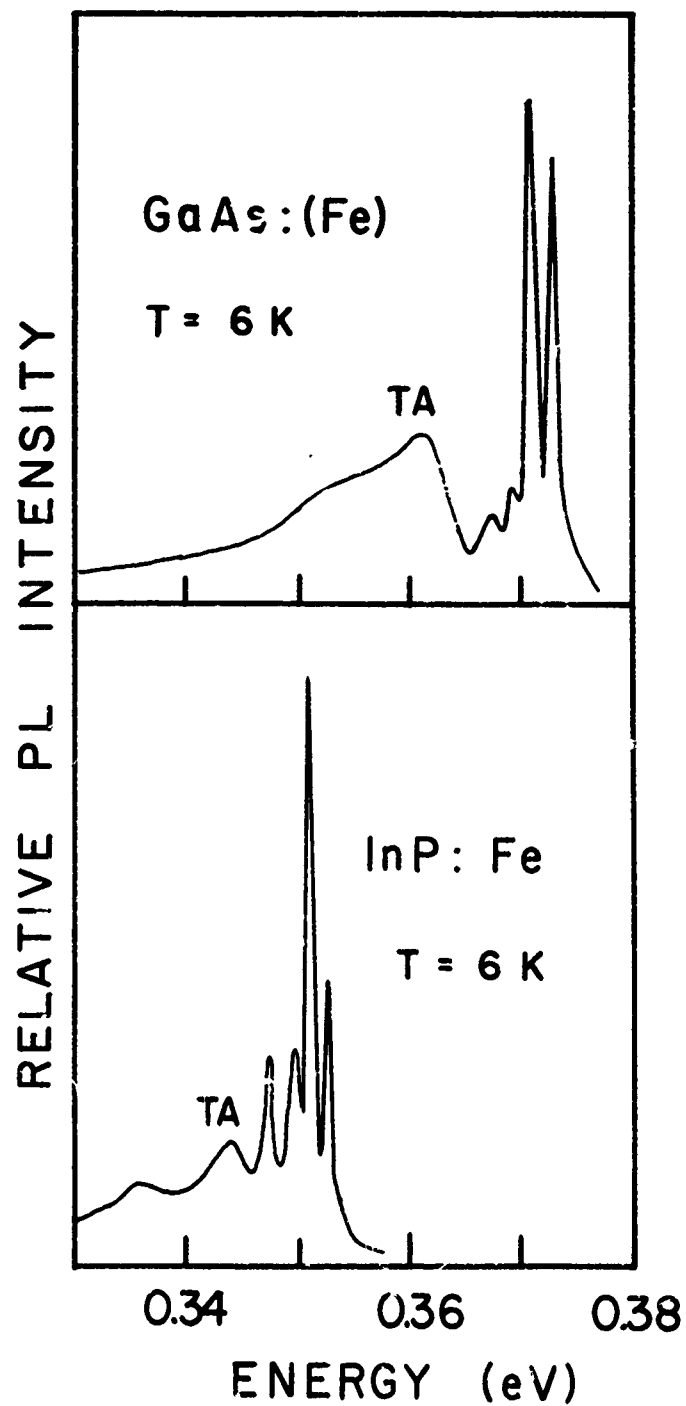
Fig. 14 — PL spectra attributed to Fe in GaAs and InP. Possible assignments of the sharp zero phonon lines to various crystal field energy levels are discussed in the text.
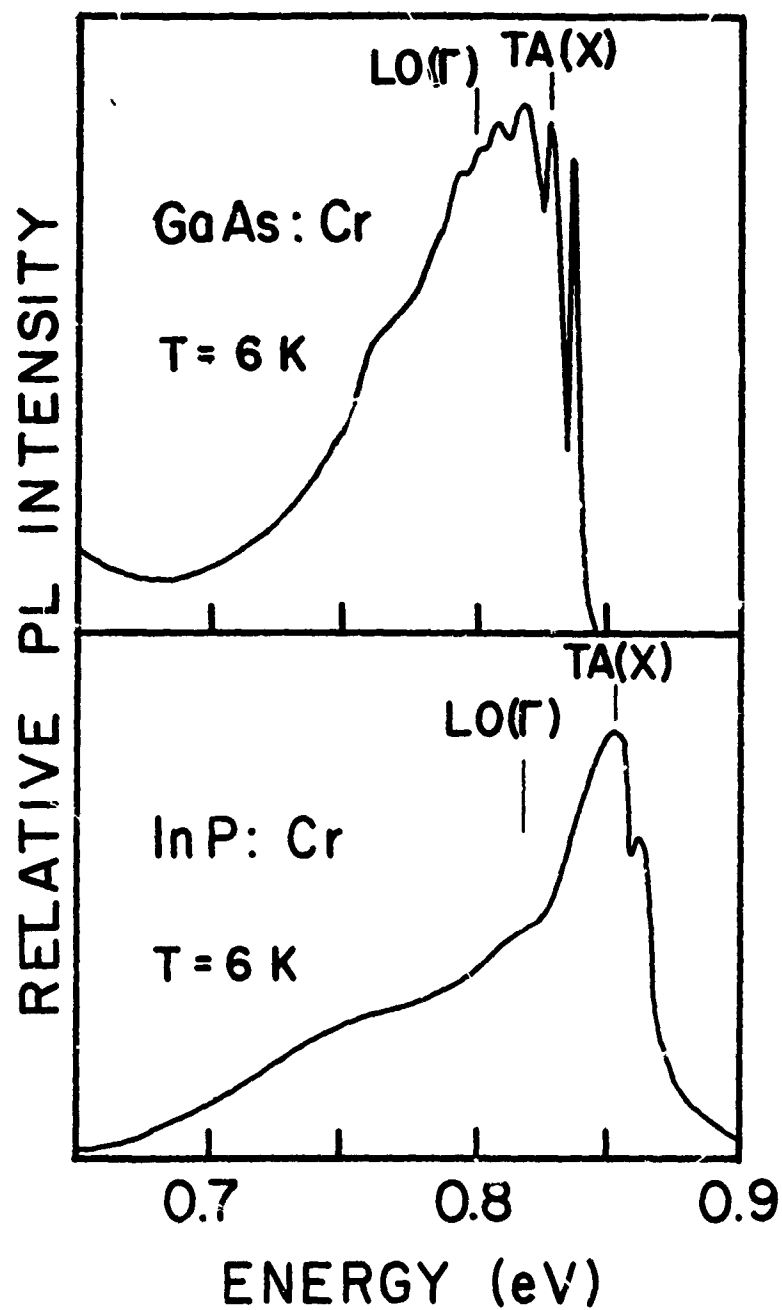
Fig. 15 — PL spectra attributed to Cr in GaAs and InP. The 0.837 eV zero phonon line in GaAs:Cr has been assigned to intra center transitions between the ^5E and $^5T_2$ crystal field levels of Cr^{2+} in tetrahedral coordination. The structure at lower energies represents phonon replicas or side bands.
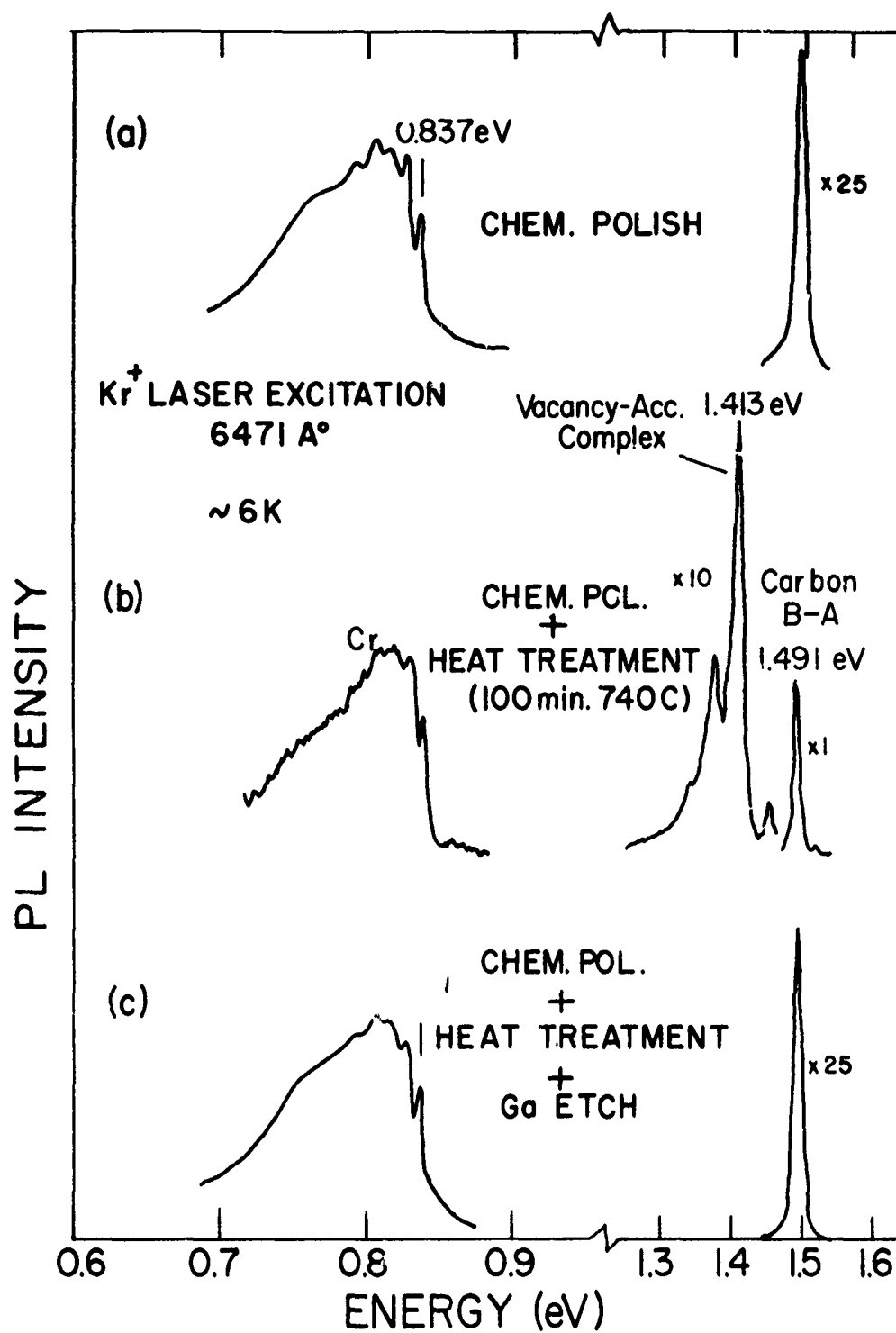
47

Fig. 16 — (a) PL spectrum in As-grown GaAs:Cr substrate. (b) PL spectrum from same GaAs substrate after heat treatment. (c) PL spectrum from heat treated substrate subjected to a Ga etch.

48

III. Bulk and Interface Properties of GaAs and InP

A. Introduction

The NELC portion of the characterization effort has progressed
in three general areas during the past year: (1) Photoluminescence
and electrical investigations of surface and interface "type-converted"
layers on semi-insulating GaAs substrates; (2) the development of an
x-ray topographic capability for the investigation of surface defects
on III-V materials; and (3) the investigation of insulating passiva-
tion layers on InP. These efforts are described in more detail in
the following sections.

B. Photoluminescence and Resistance Profiles of Surface Layers on Cr-Doped and Undoped GaAs

Principal Investigators: W. Y. Lum and H. H. Wieder, NELC

Two specimens of semi-insulating (SI) GaAs were examined: (100)-
oriented Cr-doped GaAs grown by Crystal Specialties and (100)-oriented
undoped GaAs grown by the Naval Research Laboratory. The electrical
characteristics of the two virgin n-type materials (as grown) are
almost identical: the resistivity $p \simeq 2.5\times10^8$ Ω-cm the free electron
density $n \simeq 2.5\times10^7$ cm^{-3} and the mobility $\mu \simeq 1000$ cm^2/V-sec.

Figures 17 and 18 show the PL spectral response of Cr-doped and
undoped SI GaAs, respectively, before and after they were heat-treated
at 800°C for one hour in an H$_2$ atmosphere. The spectra of the two
specimens are qualitatively the same before the thermal treatment;
both have a relatively small exciton peak at 1.517 eV and a larger
free-to-bound (F-B) peak near 1.495 eV associated with shallow
acceptors. Heat-treating these samples increases the intensity of

49

these peaks for both specimens by more than an order of magnitude. New PL peaks related to As-vacancy complexes are observed at 1.413 eV and 1.377 eV in the spectra of both samples after heat treatment. An additional peak at 1.364 eV appears in the PL spectrum after heat-treatment of the undoped GaAs. This peak may also exist in the Cr-doped GaAs spectrum, but with a much lower intensity; it is, therefore, masked by the stronger PL peak near 1.38 eV. A small shoulder is indeed present near 1.37 eV in the PL spectrum of the heated Cr-doped GaAs sample.

As shown in Table II, the half-widths of both the exciton peak and the F-B peak are significantly narrower for the undoped GaAs sample. This may indicate that it has a lower impurity (defect) concentration than the Cr-doped material. The half-widths of the PL peaks of both specimens decrease after thermal treatment. The mechanism responsible for this phenomenon is not yet known. The surface of the GaAs became conductive following heat-treatment. The charge carriers in the converted surface layer of the heat-treated NRL #II-35L specimen are holes, determined from Hall measurements made (In contacts were annealed at 400°C for 2 minutes) in a Van der Pauw configuration.

To determine the thickness of the surface converted layer of specimen NRL #II-35L, the resistance between two surface contacts was monitored as the layer was thinned in successive steps. The specimen was 4.2x4.4 mm area, and the contacts and adjoining portions of the surface were masked to expose an area 2x4.2 mm which was then thinned by anodization-stripping.

The thinning was done by anodizing the GaAs surface in a tartaric acid electrolyte with a constant current of 0.05 ma. When the voltage

50

drop across the oxide reached 6 volts, the process was terminated

and the oxide removed in dilute HF. From the data of D. L. Rode,

et al.,[1] the oxide formation is linear with a thickness of 18.6 $\overset{o}{A}$/V.

The GaAs removal is 2/3 this amount, and for the 6 volt drop the etch

step used would be 75 $\overset{o}{A}$. As a check on the step thickness, the etch

depth was measured after 12 steps. The boundary between the masked

region and the etched region was examined with a Varian Angstrometer

optical interference thickness measurement microsccpe. The surface

roughness of the specimen made it difficult to identify the desired

location, however, a definite continuous step was found and assumed

to be the boundary. This step was measured in two locations and was

$1100\overset{o}{A}$ and $1030\overset{o}{A}$ high. This agrees with the $12 \times 75\overset{o}{A} = 900\overset{o}{A}$ expected

from the anodization.

The resistance of the layer was determined from the I-V curve on

a Tectronix Curve Tracer. The data are given in Table III. The

measurements were made with the room lights out, however, the resis-

tance was so light sensitive that the last several steps were also

measured with the specimen covered. It would take 6 seconds or more

for the resistance to come to equilibrium when the specimen was

covered, indicating presence of long lifetime traps. The specimen

resistance after each etch step is shown in Figures 19 and 20. The

high dark resistance made measurements difficult so stripping was

stopped after 12 steps. There was still extreme light sensitivity

of the resistance, however, indicating that the converted surface

was not completely removed.

Van der Pauw measurements on both heat-treated SI GaAs indicate

that both surface layers are p-type. The surface layer of the

undoped GaAs sample has hole concentration $p \simeq 7 \times 10^{16}$ cm^{-3} and mobility $\mu \simeq 175$ cm^2/V-sec, while $p \simeq 1.5 \times 10^{17}$ cm^{-3} and $\mu \simeq 100$ cm^2/ V-sec for the Cr-doped sample.

It is of some interest to consider further the charge carrier transport properties of the NRL II specimen in its virgin state. Hall and conductivity measurements indicate that it is n-type with an electron density $n \simeq 2.5 \times 10^{7}$/cm^3 and a mobility $\mu \simeq 10^3$ cm^2/V-sec at room temperature. The low carrier concentration for such a mobility indicates fairly heavy compensation. D. L. Rode and S. Knight[2] have calculated the mobility dependence on free electron density and on the compensation ratio. For a mobility of $\sim 10^3$ cm^2/V-sec at room temperature and a compensation ratio of ~ 10 the electron density should be $\sim 2.5 \times 10^{17}$/cm^3. It does not seem to be realistic to allow for much larger compensation ratios while at the same time requiring the electron density to be so small. Furthermore, the mystery deepens because the origin of the compensation process is still unknown.

C. <u>X-Ray Topography</u>

Principal Investigator: A. Clawson, NELC

Reflection X-ray topography has been applied to polished GaAs and InP wafers prepared for use as substrates for epitaxial layers to determine the presence of any serious surface defects. A Berg-Barrett reflection geometry was used with copper Kα characteristic radiation to generate the X-ray image of (100) and (111)-oriented samples utilizing reflections from (440) diffracting planes. A Schwuttke scanning oscillator topography camera (Blake Industries)

with a modified sample and film holder to accommodate small specimens was used with a fine focus spot source X-ray tube with a 120 cm collimator length. The X-ray beam is a line adjustable up to 7.5 cm high and 0.5 mm wide when it reaches the specimen. The (440) reflection is at 80° to the (111) surface of InP allowing the photographic plate to be positioned parallel to the wafer to produce an undistorted diffracted image. This image is limited to that portion of the specimen illuminated by the beam; however, scanning the specimen and plate together across the beam allows large area images to be produced. The scanning reflection (440) image of a (111) B chromium-doped indium phosphide polished surface 7x9 mm is shown in Figure 21. This specimen, grown by R. L. Henry of NRL, has been chemo-mechanically polished in Bromine-methanol and shows no regions of gross defects or strain in the top 5 μm of the surface. Resolution of this image is limited by the mechanical motion of the scanning and by the graininess of the thick emulsion photographic plate. LPE growth on an InP epilayer on this substrate after a light clean-up etch in bromine/methanol showed no evidence of substrate-induced defects.

D. Insulating Layers on InP

Principal Investigators: L. Messick and D. Lile, NELC

MOS diodes were fabricated on bulk single crystal regions of InP using pyrolitically deposited SiO_2 as the insulator.[3] High frequency (1 MHz) differential capacitance measurements were then made as a function of bias, a typical example of which is shown by the solid line plot in Figure 18. Using the carrier concentration as obtained from a Hall measurement, the theoretically (Terman) anticipated C/V behavior was then calculated. This is shown by the

53

dashed curve in Figure 18. Except for the region of minority
carrier inversion, it is evident that the theoretical and experi-
mental curves are in close agreement, suggesting that there exists
at this interface a very low density of trapping states. It is
estimated that the apparent surface state density is, in this case,
$<10^{11}$ cm^{-2} eV^{-1}, and that any trapped charge that may exist in this
oxide system is below the resolution limit of the C/V measurement.

References:

[1] D. L. Rode, B. Schwartz, and J. V. DiLorenzo, Solid-State Electronics
<u>17</u>, 1119 (1974).

[2] D. L. Rode and S. Knight, Phys. Rev. <u>3B</u>, 2534 (1971).

[3] L. J. Messick, "InP/SiO$_2$ MIS Structure," accepted for publ. in
J. Appl. Phys.

TABLE II. COMPARISON OF HALF-WIDTHS OF PL BANDS

IN Cr-DOPED AND UNDOPED GaAs

Sample*	Half Width	
	exciton peak	F-B peak
NRL II-35L (before heating)	3.4 meV	5.8 meV
NRL II-35L (after heating)	3.2 meV	5.3 meV
Crystal Specialties (before heating)	5.2 meV	9.7 meV
Crystal Specialties (after heating)	3.9 meV	7.9 meV

*NRL II-35L: undoped GaAs grown by Naval Research Laboratory

 Crystal Specialties: Cr-doped GaAs grown by Crystal Specialties

TABLE III

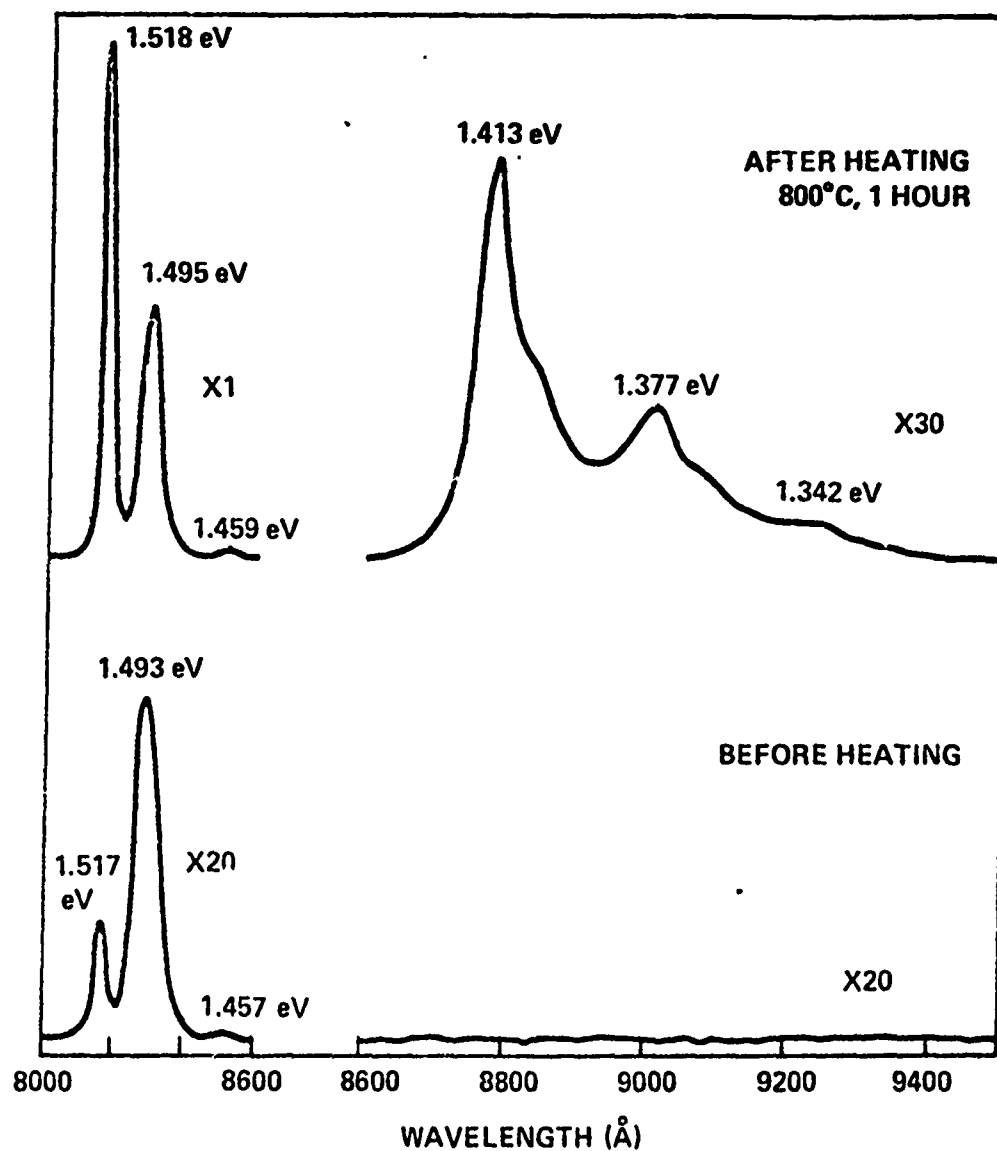| Anodization/Strip Step	Room Lights Off		Specimen Covered	
	I	V	I	V
0	.08 ma	20 volts		
1	.065	20		
2	.062	20		
3	.048	20		
4	.042	20		
5	.036	20	.005 ma	20 volts
6	.028	20	.004	20
7	.028	20	.003	20
8	.026	20	.003	20
9	.021	20	.002	20
10	.017	20	.001	20
11	.017	20	.001	20
12	.016	20	∿.0005	20

Fig. 17 — Photoluminescence spectral response at 20K of Cr-doped SI GaAs before and after thermal treatment at 800°C for one hour in an H_2 environment
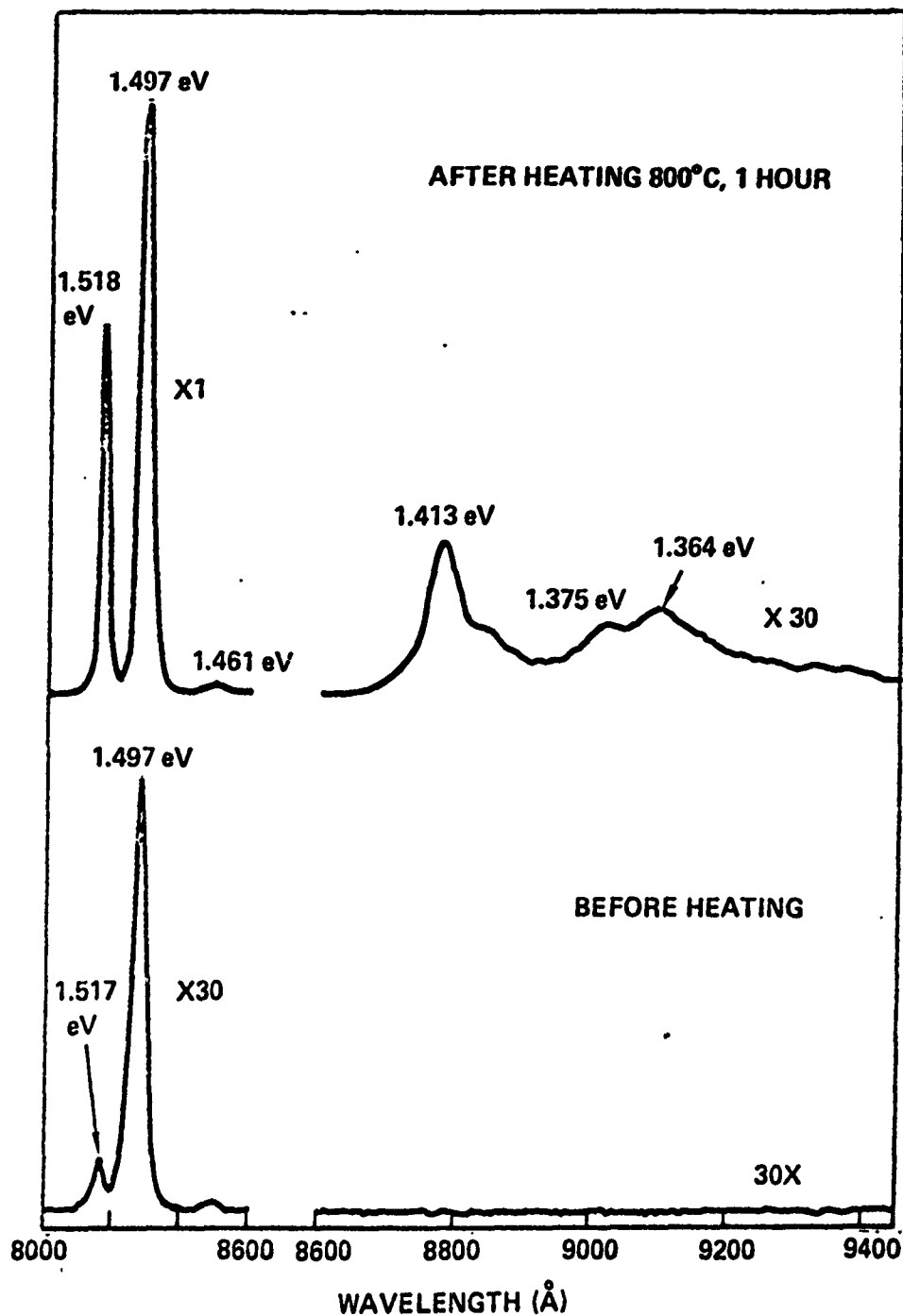
57

Fig. 18 — Photoluminescence spectral response at 20K of undoped SI GaAs before and after thermal treatment at 800°C for one hour in an H_2 environment
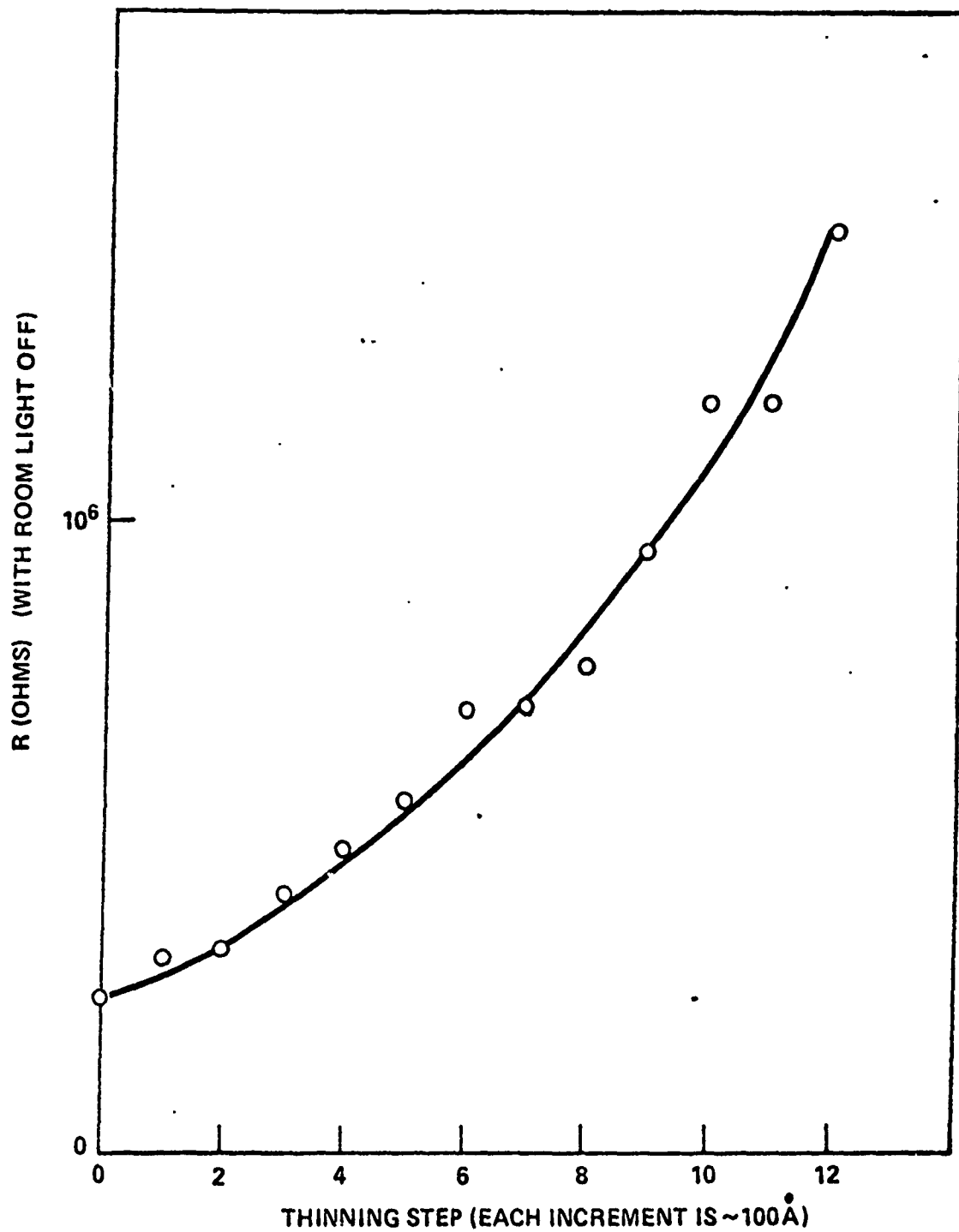
Fig. 19 — Resistance of a thermally converted surface layer of a heat-treated
GaAs wafer (NRL #-35L) following successive thinning steps; specimen ex-
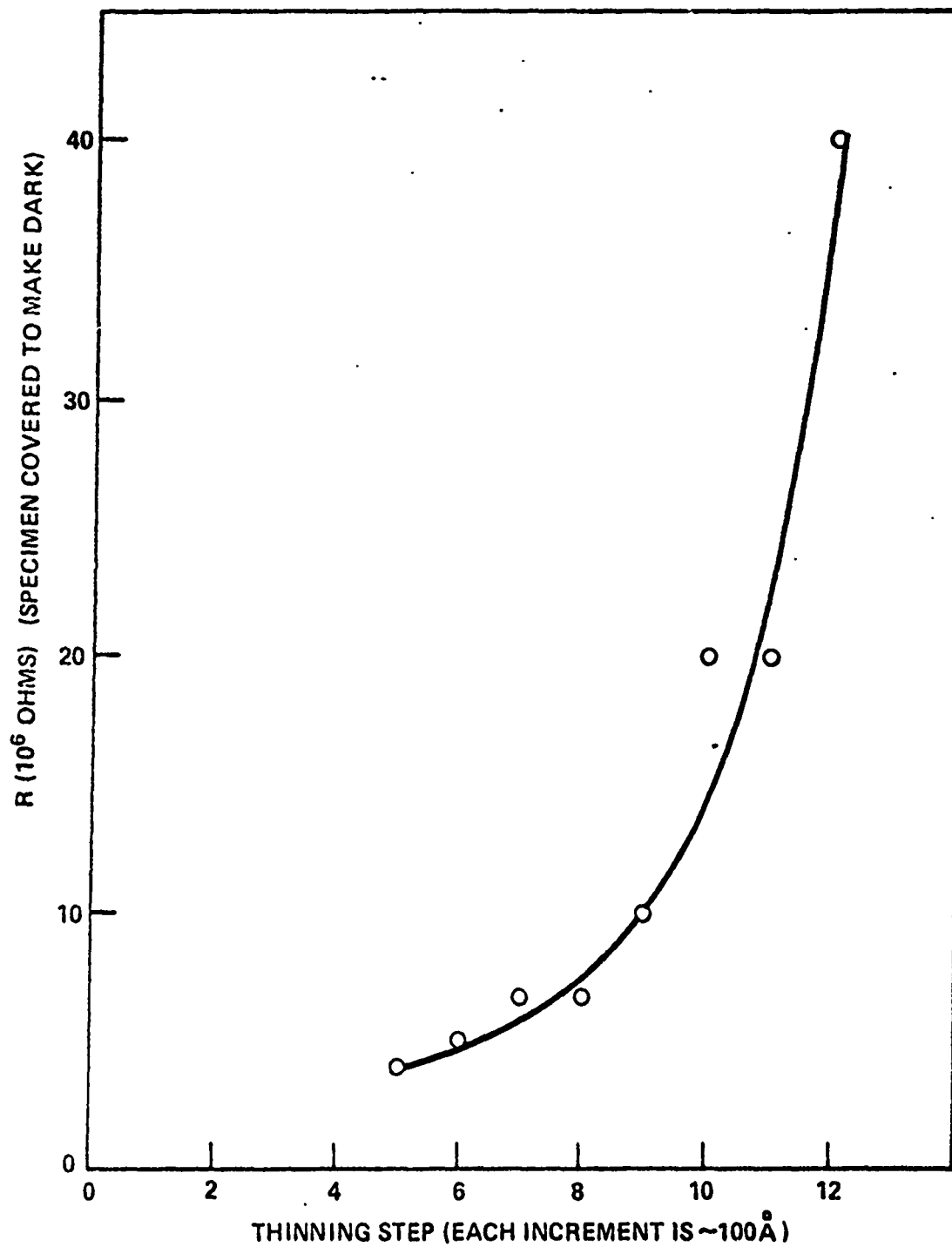posed to subdued ambient light

59

Fig. 20 — Resistance of the heat-treated GaAs wafer
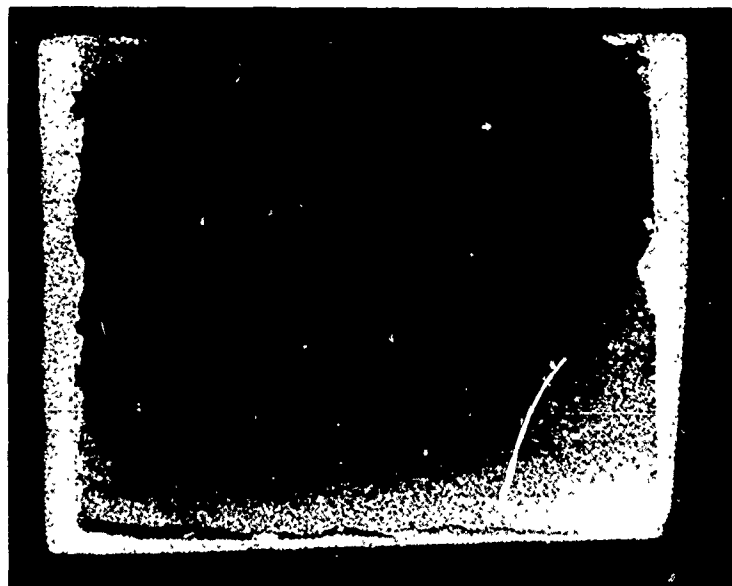in Fig. 3 with the specimen in the dark

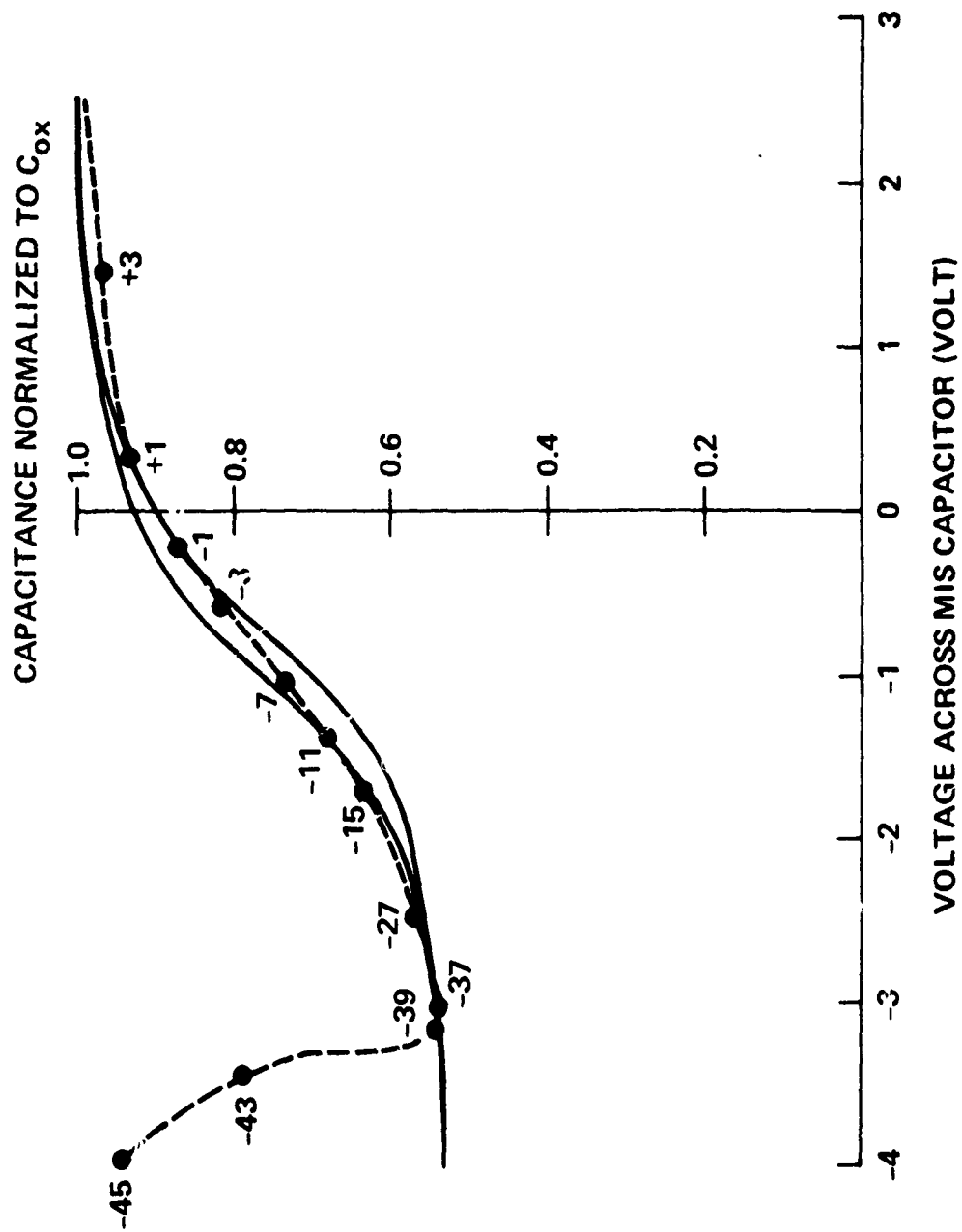Fig. 21 — X-ray topograph of NRL InP:Cr

Fig. 22 — Capacitance-voltage plot for MOS capacitor on InP. The solid circles indicate the calculated surface potentials.

DEVICE FABRICATION AND EVALUATION

1. GaAs FET Device Fabrication and Evaluation

Principal Investigator: K. J. Sleger, NRL

A. Introduction

The RF performance of the Schottky barrier GaAs FET is directly related to the properties of its thin conducting channel region and to the semi-insulating GaAs beneath. Consequently, GaAs FET structures provide for convenient materials evaluation of epitaxial and ion implanted GaAs layers intended for microwave application. For somewhat thicker GaAs layers the three terminal Gunn device provides a convenient test structure for materials evaluation. Both structures provide information related to carrier concentration, electron mobility, trapping, interfaces and variations in channel thickness.

B. Approach

Initially GaAs n-channel Schottky barrier FETs will be fabricated using conventional photolithography. Relaxed gate lengths will range from two to eight microns. Metal contacts will be evaporated using either an electron beam or resistance heating. The gate will be Al, and the source/drain contacts will be Ag/In/Ge. Figure 23 shows two FET patterns being used to define FET structures, GaAs FET material will be supplied by the Electronic Materials Technology Branch (Code 5220) and by commercial vendors. Material will be in the form of a thin epi layer of 2000 to 5000 Angstroms thick uniformly doped to 5 to 20×10^{16} cm^{-3} and grown on a semi-insulating substrate. Layer mobility should be in excess of 4000 cm^2/V. sec. As an alternate approach FET material will be generated by ion implantation of S,

63

Se into semi-insulating substrates followed by standard FET pro-
cessing into devices.

After metallization individual FETs will be mounted in RF
packages and characterized in the small signal mode over the fre-
quency range 1-10 GHz. RF performance will be related to static
characteristics, materials parameters and non-destructive measure-
ments performed independently by the Semiconductors Branch (Code
5270).

C. Status and Plans

GaAs Schottky barrier FETs have been fabricated from wafers
supplied by NRL Code 5220, Raytheon and Avantek. All FETs were
examined on a curve tracer to determine static parameters. A FET
processed from Avantek material showed a gain of 7 dB at 2 GHz.
This device had a gate length of 2 microns. FETs processed from
Code 5220 and Raytheon material have not yet been characterized at
microwave frequencies. Table IV lists the DC parameters of the
three types of FETs fabricated to date. Table V lists the measured
materials properties of the various wafers.

The theoretical g_m of 15-20 millimhos was never achieved, per-
haps because the value of R_{SD} was too large. R_{SD} consists of a
series connection of source/drain contact resistance, parasitic edge
resistance and intrinsic resistance in the channel beneath the gate.
R_{SD} was 5-6 times too large. It is believed that the large value of
R_{SD} was due primarily to poor source/drain contacts. Consequently,
in future FETs the Ag/In/Ge contact will be replaced with Au/Ge
overlaid with thick Au. The Au/Ge contact is reproducible, does

64

not tarnish and provides a lower contact resistance than does Ag/In/Ge. In addition the thick Au overlayer prevents balling of the contact during the alloy process. A systematic study of the Au/Ge/Au contact will be made to determine the metal thickness and alloying parameters necessary in order to guarantee good Ohmic source/drain contacts.

Both Raytheon and Avantek wafers produced FETs whose DC characteristics were only moderately sensitive to light from a microscope illuminator. No looping was observed. On the other hand wafers supplied by Code 5220 from early growth runs produced FETs that were dramatically sensitive to light, showing no transistor action (gate voltage modulation of drain current) unless intense light was present. The light-induced transistor characteristic was dominated by looping. This unusual behavior may be related to contact phenomena, traps in the GaAs or interface effects at the epi-substrate interface. Backside gating experiments will be performed as the first step in determining the physical processes involved with this light sensitivity.

Al was used for the gate metal in nearly all devices. A Cr/Au gate was used for the FET characterized at microwave frequencies. Cr/Au adheres to GaAs much better than does Al and was only used to enhance the chances of successful FET fabrication. Cr/Au is highly unattractive from a reliability standpoint. Many problems were encountered in trying to get Al to stick to GaAs and, thus, to produce consistent gate/source I-V characteristics. It is believed that the ability of Al to stick to GaAs is related to

GaAs surface cleanliness and Al_2O_3 formation during evaporation. In a systematic study it was found that gate definition using a lifting technique leaves S, C, Cl and O contaminants in the channel region. These contaminants are presumably the result of incomplete photoresist removal, and may decrease the sticking ability of Al. Currently a wet etch process is being developed to define the Al gate. This should enhance Al sticking since the channel region will not be exposed to photoresist. Also Ta and Ti/W are being investigated as gate metallizations.

Several Cr doped wafers of semi-insulating GaAs were implanted with sulfur and processed into FET structures. Current saturation of the source drain characteristic was not observed, presumably because implants were too deep. Low resistance ohmic contacts could not be made to implanted layers. More wafers are being implanted and will be carefully characterized before processing into FETs. The ion implanted FET capability will be necessary to provide device/materials analysis of the high quality semi-insulating GaAs now being produced by Code 5220 as a part of the materials development program. It is to be noted that this portion of the program is being supported by NRL 6.1 funds.
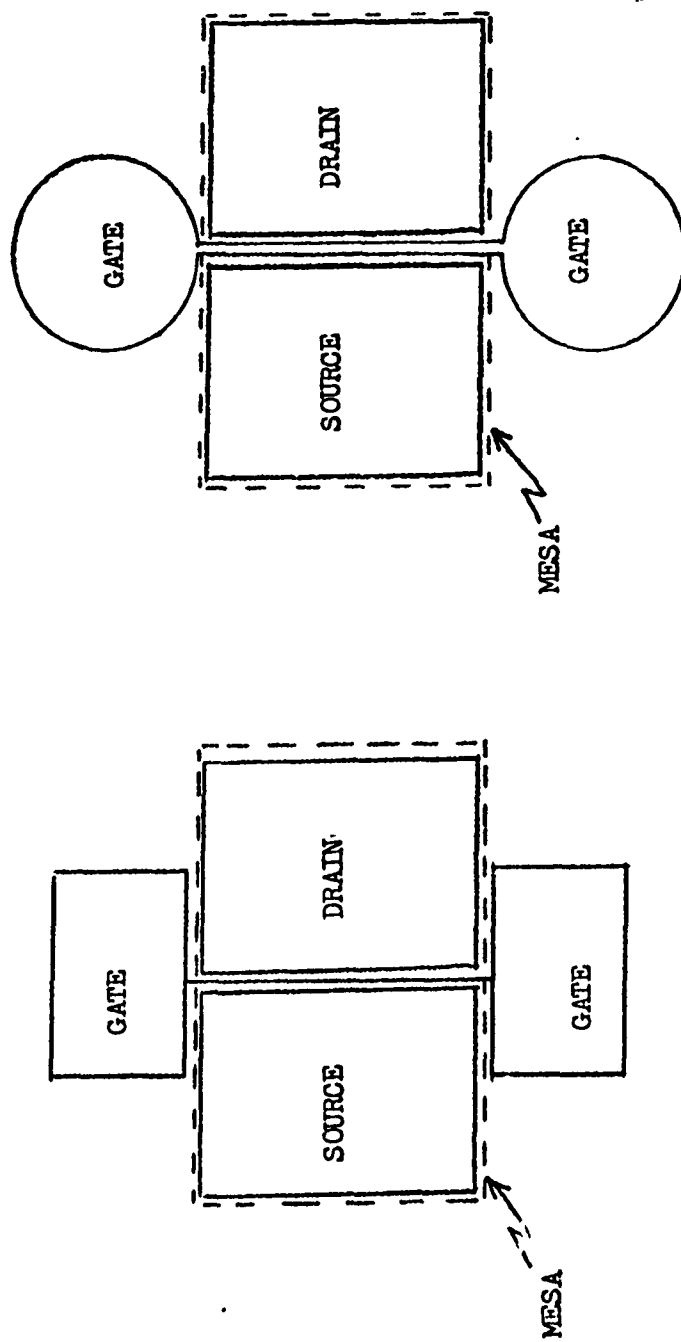
TABLE IV FET DC CHARACTERISTICS

WAFER SOURCE	I_{dss}	V_p	g_m	R_{SD}	LIGHT SENSITIVITY
	mA	Volts	millimhos	ohms	
CODE 5220	12.0	6.0 (with light)	5 (with light)	50	No transistor action without light
RAYTHEON	4.5	2.0	5	60	Moderately sensitive to light
AVANTEK	10.0	1.5	7	90	Moderately sensitive to light

67

TABLE V WAFER MATERIAL PROPERTIES

WAFER SOURCE	EPI LAYER THICKNESS MICRONS	EPI LAYER CARRIER CONCENTRATION CM^{-3}	EPI LAYER MOBILITY $CM^2/V \cdot sec$	BUFFER LAYER
CODE 5220	0.3–0.4	4–7×10^{16}	3000–5000	NO
RAYTHEON	0.26	1×10^{17}	4000	NO
AVANTEK	0.18	1×10^{17}	not measured	10 microns

NOTE: All substrate material is Cr doped
semi-insulating GaAs

(b) Gate Lengths of 2, 4, 6, and 8 microns

(a) Gate Lengths of 1.0, 1.2, 1.5, and 2.0 microns

Fig. 23 — NRL FET geometries. (a) Fine geometry; (b) Relaxed geometry.